VIABILITY AND REPRODUCIBILITY OF ADDITIVELY MANUFACTURED SHAPE MEMORY ALLOYS AND HIGH TEMPERATURE SHAPE MEMORY ALLOYS

A Thesis

by

JOEL J. SAM

Submitted to the Office of Graduate and Professional Studies of
Texas A&M University
in partial fulfillment of the requirements for the degree of

MASTER OF SCIENCE

Chair of Committee,	Ibrahim Karaman
Committee Members,	James Boyd
	Ankit Srivastava
Head of Department,	Ibrahim Karaman

December 2018

Major Subject: Materials Science and Engineering

ABSTRACT

Shape memory alloys (SMAs) are metals that can "remember" the shape they were in before deformation and can return to that shape upon heating. These alloys have a structure that changes based on applied stress and temperature and are promising candidates for solid-state actuators in the robotics and aerospace industries.

Conventionally manufactured SMAs must undergo further processing to be formed into desired structures. With further processing there is a greater chance of introducing inclusions such as oxygen and carbon, which greatly affect the transformation temperatures of SMAs, as well as forming cracks and other structural defects. Additive manufacturing (AM) of SMAs combines alloy production and forming into a single step, reducing extraneous processing steps. AM SMAs do not currently perform as well mechanically as their conventionally manufactured counterparts. Tensile shape memory actuation was characterized for nickel-titanium (NiTi) SMAs fabricated using the laser powder bed fusion (L-PBF) AM process and two different sets of processing parameters in order to determine the viability of AM SMAs. While reversible tensile shape memory behavior was observed in both cases, the specimens fabricated with a shorter hatch spacing exhibited higher transformation temperatures, lower actuation strain, and lower irrecoverable strain compared to the specimens fabricated with wider hatch spacing. The actuation strain of the L-PBF samples was lower than that of conventionally manufactured NiTi SMA specimens.

High temperature shape memory alloys (HTSMAs) are a class of SMAs that have elements added to increase their transformation temperatures for use in high-temperature environments to prevent accidental actuation. The nickel-titanium-hafnium (NiTiHf) system has shown significant promise as an HTSMA with higher strength and work output than NiTi. Batches of NiTiHf produced in previous studies have shown variation in fatigue life and transformation temperatures despite similar compositions. A parameter called "actuation potential" was created to quantify hypothetical performance of each batch in actuator applications. Carbide content, precipitate size, stress-strain curves, stress-temperature phase diagrams, and transformation strain data from four batches of NiTiHf were used to search for the underlying causes of batch-to-batch variation in NiTiHf. Correlations of carbide content and precipitate size with actuation potential were observed, and hypotheses as to why these variations affect performance are proposed.

ACKNOWLEDGEMENTS

I would like to thank my committee chair, Dr. Ibrahim Karaman, for welcoming me into his lab as a senior undergraduate student with no prior experience. He gave me projects to work on that taught me the value of materials science research and the practical applications of shape memory alloys. As I pursued graduate studies, he funded my research, taught me to think like a scientist, and gave me opportunities for technical presentation and publication. I am incredibly grateful for his mentorship.

Thanks also go to my friends and colleagues in the MESAM laboratory for their technical assistance in my research. Without their assistance, my skill in material science research methods and experimental procedures would have lacked. Specifically, I would like to thank Ceylan Hayrettin, Omer Karakoc, Brian Franco, Nazim Babacan, Nick Barta, Tejas Umale, Hande Ozcan, and Michael Elverud for their instruction.

I am grateful for the department faculty and staff of Materials Science and Engineering for making my academic experience in graduate school at Texas A&M University memorable and intellectually rewarding. Specially, I would like to thank Jules Henry for serving as my academic advisor, in addition to Dr. Ankit Srivastava and Dr. James Boyd for serving on my committee.

My college experience would have been impossible without the dear friendships and mentorships I had during my six years at Texas A&M. I would specifically like to thank Mickey Gashaw, Simon Yau, Daniel Walls, Adam Kier, Joel Nakamura, Joseph Dunne, Josh Cheung, Scott Sawyer, Joshua Hargis, Caleb Davis, Hannah LeGare, Jo

CONTRIBUTORS AND FUNDING SOURCES

Contributors

This work was supervised by a thesis committee consisting of Professor Ibrahim Karaman, Professor James Boyd of the Department of Aerospace Engineering and Professor Ankit Srivastava of the Department of Materials Science and Engineering.

Some content from Chapter 1 was adapted from work co-written by me, Olga Eliseeva, Benjamin Young, and Alexander Demblon. In Chapter 3, some DSC data, all TEM data, and the parametric study were performed and provided by Brian Franco. In Chapter 4, some DSC and fatigue experiments were performed by Sam Brackett, and the TEM, SEM, and fatigue data was provided by Omer Karakoc.

Funding Sources

NOMENCLATURE

A	Austenite
$A \to M$	Austenite to Martensite transformation
A_f	Austenite finish temperature (°C)
AM	Additive Manufacturing
A_p	Austenite peak temperature (°C)
A_s	Austenite start temperature (°C)
BSE	Backscattered Electron
DSC	Differential Scanning Calorimetry
EDM	Electrical Discharge Machining
EDS	Energy Dispersive Spectroscopy
Hf	Hafnium
$HTSMA$	High Temperature Shape Memory Alloy
M	Martensite
$M \to A$	Martensite to Austenite transformation
M_f	Martensite finish temperature (°C)
M_p	Martensite peak temperature (°C)
M_s	Martensite start temperature (°C)
Ni	Nickel
OM	Optical Microscopy
PE	Pseudoelastic Effect

SEM	Scanning Electron Microscopy
SIM	Stress-Induced Martensite
SMA	Shape Memory Alloy
SME	Shape Memory Effect
SMM	Shape Memory Material
T	Temperature (°C)
TEM	Transmission Electron Microscopy
Ti	Titanium
ΔT	Temperature Change (°C)
ε	Strain (%)
ε_{act}	Actuation Strain (%)
ε_{irr}	Irrecoverable Strain (%)
ε_{trans}	Transformation Strain (%)
σ	Stress (MPa)

TABLE OF CONTENTS

Page

LIST OF FIGURES

xii

LIST OF TABLES

Page

CHAPTER I

INTRODUCTION AND OBJECTIVES[1]

History of Shape Memory Alloys

In 1932, Arne Olander first discovered that gold-cadmium alloys could be plastically deformed and then returned to an original shape when heated [1]. In 1951, L. C. Chang and T. A. Read further confirmed this discovery by finding that a gold-cadmium alloy that was heated with and without applied stress showed significant changes in resistivity at different temperatures [2]. In Chang and Read's experiment, two distinct solid phases were observed, and motion pictures were taken that showed the changes in surface contour during transformation between the phases. Stress-strain curves generated through a bending test showed unexpected behavior during unloading, indicating that the two phases showed distinct mechanical properties. Documentation of this phenomenon was published and materials showing this behavior were subsequently called "shape memory alloys".

In 1962, the shape memory effect was discovered accidentally in nickel-titanium by William Buehler [3], [4], while searching for a strong high-temperature alloy for use in missile nose cones. Upon observing the shape memory effect in this material and anticipating its potential use in thermo-mechanical actuation, the material was named

---

"NiTiNOL", in honor of the Naval Ordnance Laboratory where it was discovered. NiTiNOL, or binary nickel-titanium, evolved into a burgeoning field of research for metallurgists, and development of practical uses of NiTi increased significantly over the coming years due to its high strength, corrosion resistance, pseudoelasticity and shape memory behavior.

Nickel-titanium-based materials continue to be the most commonly used SMAs, and they have the potential to perform well in many critical applications; including, but not limited to those in the automotive, aerospace, and biomedical industries [1], [5], [6]. Some pivotal applications of SMAs over the years include Raychem's CryoFit™ "shrink-to-fit" pipe coupler for fighter jets, George B. Andreasen's orthodontic bridge wires, and Boeing's variable geometry chevron [7]. Shape memory alloys are capable of withstanding great loads during transformations, and can achieve large transformation strains, making them especially useful for actuation applications.

Research into the addition of ternary elements to NiTi has expanded the reach of SMAs to both low-temperature and high-temperature applications [6], and other alternative SMAs such as magnetic SMAs, shape memory polymers, shape memory ceramics, and composites have been studied [1]. Additionally, research has been conducted to investigate alternative manufacturing methods for SMAs, such as additive manufacturing. This work will focus on two burgeoning areas of SMA research: high-temperature SMAs and additive manufacturing of SMAs.

Shape Memory Effect

Shape memory alloys (SMAs) are materials that demonstrate the shape-memory effect (SME) and pseudoelastic (or superelastic) effect (PE) [8]. The shape memory effect is where an SMA undergoes a phase transformation as a function of temperature, and the pseudoelastic effect is where the same transformation occurs due to applied stress. SMAs can return to an original shape after deformation if a large enough change in temperature is applied.

The shape memory effect is due to a reversible, diffusionless phase transformation from austenite (the high-temperature phase) to martensite (the low-temperature phase). During cooling or applied stress, the material begins transforming to martensite (which has a monoclinic B19' crystal structure) at a particular temperature (M_s) and finishes at another temperature (M_f). In the martensite state, any applied stress causes reorientation, or de-twinning, of the martensitic crystal structure, which appears to be plastic deformation. Upon re-heating, the material begins transforming to austenite (cubic B2 crystal structure) at A_s and finishes at A_f, and during this transformation the material recovers its original shape. In this way, a shape memory alloy can "remember" the shape of its austenitic state.

The transformation temperatures of an SMA can be measured in accordance with changes in the specific heat flow of the material. The amount of heat flow in the "forward" transformation (austenite to martensite) is different from that of the "reverse" transformation (martensite to austenite). Due to this hysteresis in the material, a certain

amount of mechanical energy is lost each time the material is cycled between the two phases. Because the martensitic transformation occurs due to a cooperative shearing of atoms, the mechanical state of the microstructure also influences transformation. By changing the stress state, the transformation temperatures of the material can be influenced, and the transformation temperatures typically increase as a function of applied stress.

When mechanical energy is imparted to the material in the form of applied stress, the martensite will twin, or reorient, in directions that are favorable based on the applied forces [9]. Because of this difference in symmetry, when the material is then heated, the martensite transforms into austenite, and goes back to the high-symmetry phase, where there is only one configuration of crystals. In this way, the material returns to its original, high symmetry orientation from its low symmetry orientation. Figure 1 shows how such a transformation can take place [6].
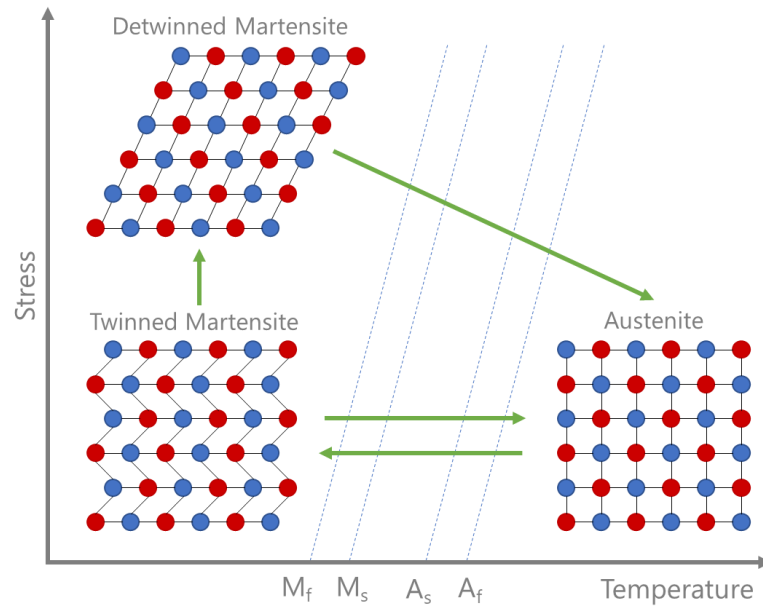
Figure 1. Phase diagram showing the crystal structures of the one-way shape memory effect

A stress vs. temperature phase diagram, shown in Figure 2, differentiates between the two phases and delineates the transformation landscape. As stress level increases, the transformation temperatures shift to higher values. The slope of M_s as a function of stress is called the Clausius-Clapeyron slope, since it is a formulation of the Clausius-Clapeyron relation from thermodynamics. For SMAs, the Clausius-Clapeyron relation can be put in the following terms [10]:

$$\frac{d\sigma}{dT} = -\frac{\rho \Delta S}{\varepsilon_t} = -\frac{\rho \Delta H}{T_0 \varepsilon_t}$$

Where dσ is the change in critical stress, dT is the change in temperature, ΔH is the transformation enthalpy, T_0 is the equilibrium temperature, and ε_{tr} is the transformation strain.

5

Two other lines of interest on the stress-temperature phase diagram are the

Martensite Reorientation (σ_{MR}) and Martensite Yield (σ_{MY}) lines. When an SMA is

completely in the martensite phase, the stress-strain curve will have two yield points:

one stress plateau where the martensite crystals reorient in a direction favorable to the

applied force (σ_{MR}), and another stress plateau showing plastic deformation (σ_{MY}), which

is a phenomenon that occurs in virtually all metals.
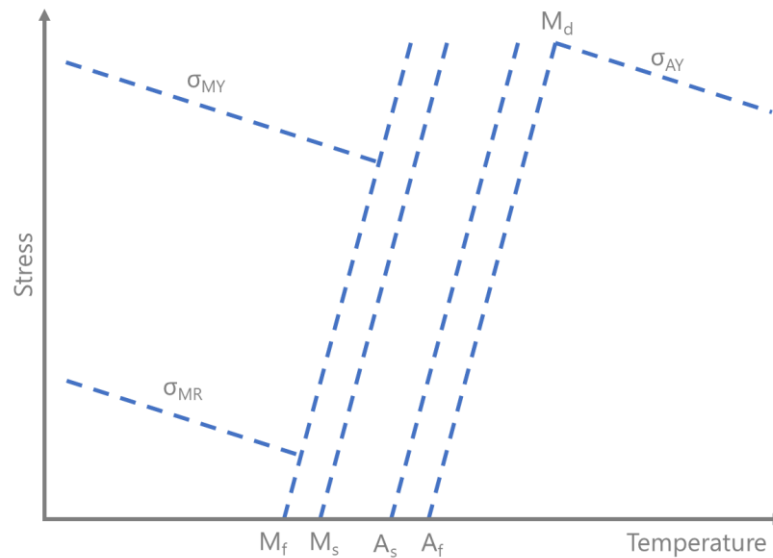
Figure 2. Stress-temperature phase diagram showing reorientation and yield lines

For SMAs, there is a temperature called M_d, above which the material no longer

transforms from austenite to martensite under applied stress. Above M_d, a permanent

shape for the austenite phase can be set via plastic deformation.

For shape memory alloys, stress-strain curves look distinctly different in martensite, austenite, and above M_d. Representative stress-strain curves, along with points of interest, are shown in Figure 3. The first stage is reversible, elastic deformation, followed by a stress plateau, either due to reorientation/detwinning in martensite (σ_{MR}) or transformation from austenite to martensite due to stress (σ_{SIM}). Next, the reoriented or stress-induced martensite phase undergoes elastic deformation, followed by another yield point for plastic deformation of martensite. For high-temperature shape memory alloys, there is significant hardening in martensite, masking the martensite yield point.
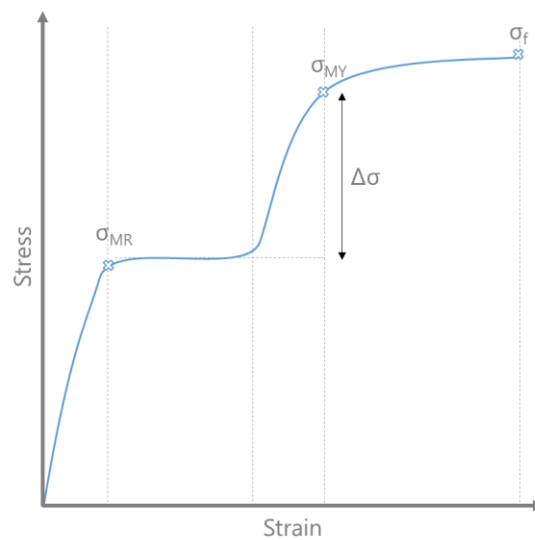
Figure 3. Stress-strain curve of a shape memory alloy in martensite

Thermo-mechanical Properties of SMAs

An isobaric heating-cooling test cycles the material between austenite and martensite temperatures under a constant load to measure the amount of actuation strain the SMA can achieve. The experiment is typically conducted under multiple stress levels to evaluate the shape memory actuation behavior as a function of stress and generate a stress-temperature phase diagram.

Each curve of the isobaric heating-cooling diagram has three distinct strains that can be measured. The transformation strain (ε_{tr}) is the total strain caused by the transformation from austenite to martensite during cooling and is the sum of actuation strain and irrecoverable strain. The actuation strain (ε_{act}) is the amount of strain recovered by the shape memory effect upon re-heating to austenite and is that most useful value for evaluating actuator applications of a particular shape memory material. The irrecoverable strain (ε_{irr}) is the amount of strain not recovered upon heating (ε_{tr}- ε_{act}), which is undesirable for thermo-mechanical applications.
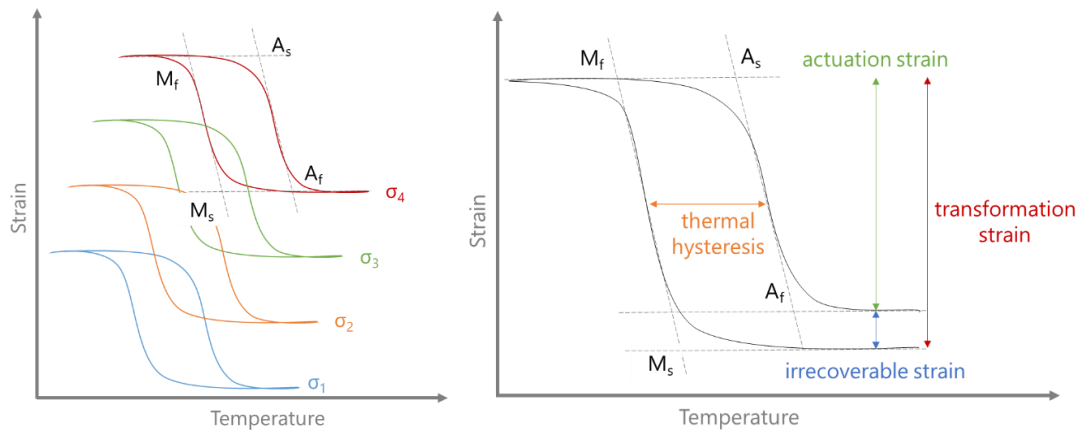
Figure 4. a) Strain-temperature diagram of a four-cycle isobaric heating-cooling experiment. b) Strain measurement of an isobaric heating-cooling cycle

Transformation strain generally increases as a function of stress, until a saturation point is reached for the amount of oriented martensite [11], where transformation strain reaches a maximum. A strain-stress diagram (Figure 5) shows the amount of transformation, actuation, and irrecoverable strain at each stress level, and it is useful for determining the viability of a shape memory materials for actuation applications.
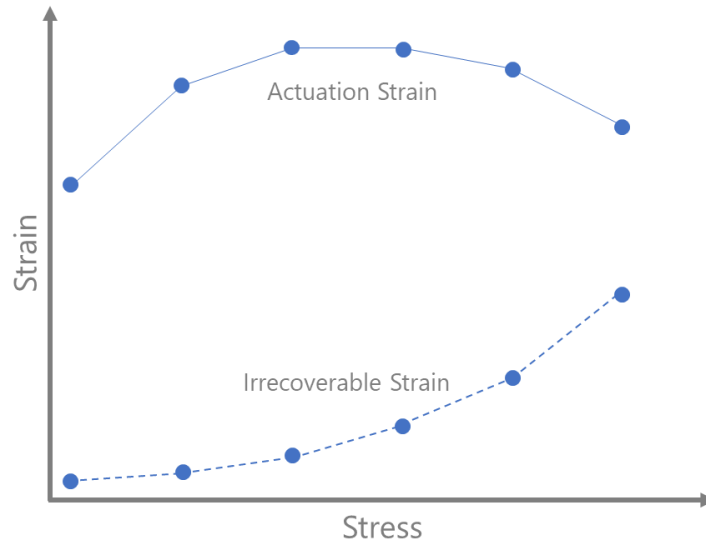
Figure 5. Strain-stress diagram of a shape memory alloy

Isobaric heating-cooling data can also reveal thermal hysteresis information. Thermal hysteresis is governed by energy dissipated by frictional work and/or elastic strain energy [11]. High energy dissipation reflected by thermal hysteresis decreases efficiency of SMAs in actuator applications. Optimal aging conditions can result in a strong matrix and low thermal hysteresis, which is ideal for strong efficient SMA actuators [11].

The M_s temperatures extracted from isobaric heating-cooling data can be used to calculate the Clausius Clapeyron relation ($\frac{d\sigma}{dT} = -\frac{\rho\Delta H}{T_0\varepsilon_t}$), since the M_s temperature indicates the critical stress for the start of forward transformation [11].

The points of interest from the isobaric heating-cooling curves and the stress-strain curves (Figure 3) across a range of temperatures can be combined to generate a stress-temperature phase diagram, as shown in Figure 6. The difference between martensite reorientation stress and stress induced martensite (σ_{SIM} - σ_{MR}) is important in quantifying the effect of processing and/or microstructural parameters on cyclic stability [12].
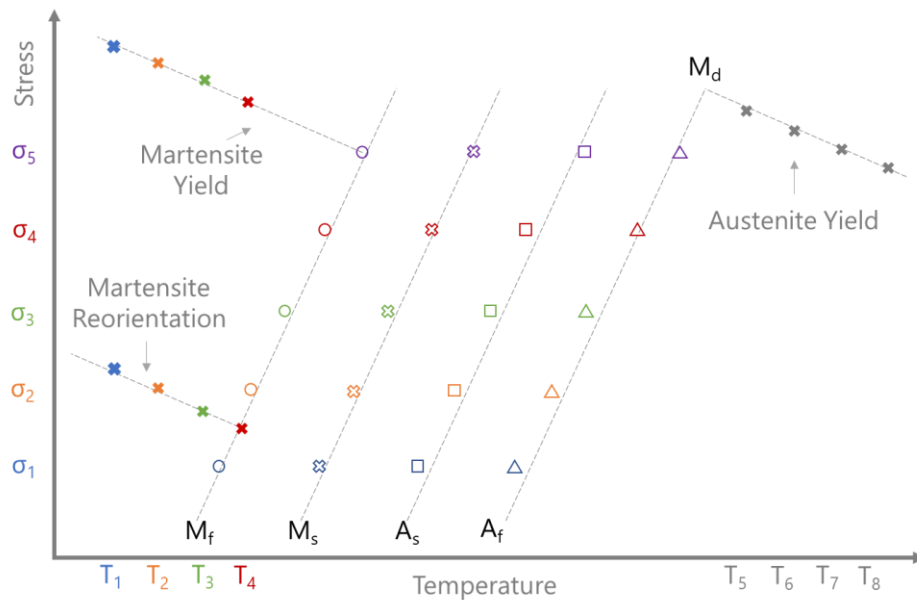
Figure 6. Stress-temperature phase diagram built from isobaric-heating cooling curves and stress-strain curves

Additive Manufacturing

In recent years, additive manufacturing (AM), colloquially known as "3D printing", has become a novel manufacturing method for a variety of materials, primarily

for rapid manufacturing of prototype parts from polymers. However, the unique advantages offered through additive manufacturing principles can open the door for a lucrative new manufacturing method for metals.

Research and development into additive manufacturing of metals has attracted the aerospace and medical technology communities [13], [14], with precise parts made through AM already commercially available. AM allows for fine control of geometry, composition, and more recently, microstructure, all of which are extremely important in the delicate systems where shape memory alloys are applied. There are two main types of additive manufacturing methods for metals: direct deposition and laser powder bed fusion.

Direct deposition is characterized by metallic powder flowing directly from hoppers into an energy source, where a liquid metal droplet is formed and quickly solidifies in place [14]. The energy source then moves to a different location and the process continues. Direct deposition is uniquely positioned in the additive manufacturing world to deal with high throughput fabrication, mending existing parts and precisely controlling composition. The unique advantage of direct deposition is that different metal powders can be deposited separately, opening the door for unique alloys and composition gradients. In the context of shape memory alloys, functionally graded materials can be developed [15], where different areas of the specimen have different shape memory properties.

Laser powder bed fusion (L-PBF) is another additive manufacturing method for metals, whose name originates from the bed of metallic powder that contains the printing medium. The mechanisms involved in L-PBF (also known as selective laser melting, or SLM) are shown in Figure 7. In this process, a roller deposits a layer of metallic powder onto a print bed, and the powder is selectively melted by a laser. Another even layer of metallic powder is rolled on top of the melted layer, continuing the process until the desired part is completed and can be removed from the un-melted powder [14]. The main drawback to a powder bed system is that only single compositions can be printed at a time, limiting the ability to change or control the composition during the printing process, which may be desirable in composition sensitive applications such as shape memory alloys. As a result, feedstock powder must be pre-alloyed; however, input parameters can be adjusted to tailor composition indirectly.
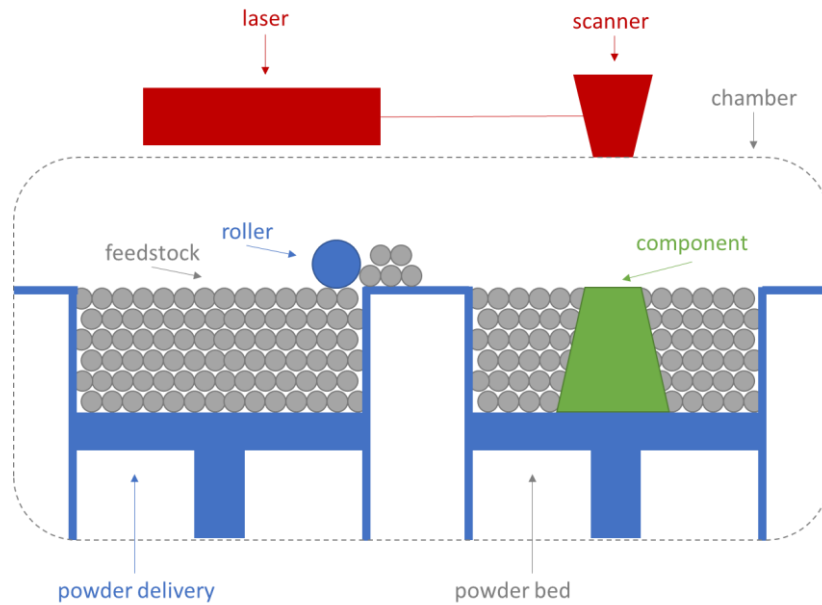
Figure 7. Laser powder bed fusion process

Literature Review

Additive Manufacturing of SMAs

The application potential of NiTi is severely limited by the difficulty of manufacturing it using conventional methods such as casting, machining, or powder metallurgy, especially when parts with intricate shapes are needed. This is attributed to many factors, including high reactivity, high strength, and poor formability [15]–[20]. To date, the majority of manufactured NiTi parts have been limited to simple geometries such as wires, tubes, and sheets [15].

Additive manufacturing techniques can help address these challenges and enable the fabrication of NiTi parts with complex geometries that cannot be easily produced

using conventional methods, such as porous scaffolds for biomedical applications [5]. In addition to producing complex geometries, AM offers the unique capability of tailoring properties in different locations within the same part [21], [22]. For example, since shape memory properties are dependent on transformation temperatures, by controlling the AM processing parameters, a part can be built with different transformation temperatures in different locations of the part, eventually leading to location specific properties [21].

However, there are still many problems in additive manufacturing that make large-scale production of shape memory alloys difficult. A few of these problems include porosity, lack of fusion defects, residual stresses, differential evaporation, and segregation of composition. These problems cause local changes in composition and/or stresses, which can change the ability for the martensitic transformation to take place [9], thereby limiting the usefulness of the shape memory alloy.

Porosity and lack of fusion are one of the most common flaws in additively manufactured parts [23], and these flaws can be caused by failure to control thermal energy input into the system. Too much thermal energy causes evaporation of the metal, and not enough thermal energy causes the powders not to fuse [23]. For a load-bearing part, pores can become localized stress concentrators for defects in the parts. Since not all pores are perfectly spherical, cracks can easily initiate from their edges and cause internal stresses in the additively manufactured product. While local stress concentrations may not result in direct part failure, they can result in changes to the

percentage of martensitic transformation that occurs, since the martensitic transformation can be stress-induced [9].

Stress can be induced into an additively manufactured part in ways other than material porosity. Parts are generally printed on build plates, and these plates are made of the same material being printed. However, these plates are large and act as thermal sinks for the additively manufactured part. These large thermal sinks increase the thermal gradient in the part as it is being built and can cause the part to be thermally shocked as it is repeatedly heated and cooled, which can result in residual stresses propagating into the additively manufactured parts, which again changes the point at which the martensitic transformation occurs [24].

Another common problem in additive manufacturing is differential evaporation, when the difference in boiling points of metals causes the preferential evaporation of one element over another, effectively changing the overall composition of the part [25]. This can be detrimental to SMAs due to the high dependence on the correct ratio of constituent elements. In well-studied SMA systems such as NiTi, the ratio between nickel and titanium is extremely important, and even a 1% change will change transformation temperatures significantly. During the additive manufacturing process nickel and titanium evaporate at different rates due to their different evaporation points [25], leading to varying nickel-titanium ratios before and after printing.

Yet another problem in additive manufacturing that causes compositional change is local segregation of elements [25]. Even though the additive manufacturing process

consists of rapid solidification, and therefore much of traditional kinetics does not apply, there is still a large amount of compositional segregation that occurs. This separation occurs as the laser moves across the powder bed resulting in stirring within the weld pool [25]. This stirring results in elements of different atomic mass to preferentially separate to the edges or center of the weld pool, causing inhomogeneity within each individual weld pool [25]. This inhomogeneity creates challenges for SMAs, since it can cause variations in transformation temperatures or cause precipitates to form that increase brittleness and decrease fatigue life.

There is a substantial amount of studies in literature on the fabrication of NiTi SMAs using AM technology, with emphasis on L-PBF processes [15], [17], [19], [21], [22], [26]–[30]. Many aspects of AM fabricated NiTi have been investigated, including mechanical properties [17], functional properties [22], and microstructure [28], [29], among others. In terms of mechanical properties, the majority of prior studies have focused on studying compressive shape memory actuation or superelastic responses [22], [26], [29], [30]. In contrast, tensile actuation of AM-fabricated NiTi has not been adequately addressed [30]. Characterizing tensile actuation is important since many applications of NiTi shape memory actuators operate under at least partial tension (such as bending) and the remnant porosity is one of the defects that may persist in AM parts and negatively affect the tensile properties, which may not have a notable effect on the properties under compression.

High Temperature Shape Memory Alloys

Binary NiTi SMAs are limited to applications below 100°C because of their low martensitic transformation temperatures [31], and higher actuation temperatures are required for many applications [6]. There is a class of SMAs called high-temperature shape memory alloys (HTSMAs), which are especially useful in oil and gas, automotive, and aerospace applications where high ambient temperatures require higher actuation temperatures than conventional SMAs. HTSMAs have the added benefit of higher strength and work output compared to binary alloys. These alloys are typically produced by adding ternary elements to NiTi, increasing transformation temperatures while retaining mechanical and functional properties [11]. Ternary elements such as Hf, Zr, Pd, Pt, and Au successfully increase transformation temperatures, but can hinder ductility and processing, and often drive up material cost [6], [31].

NiTiHf shows excellent promise as a relatively inexpensive ternary SMA system. Hf appears to have greater success than other elements such as Pd or Au in increasing NiTi transformation temperatures while maintaining lower production cost [11], [32], [33]. However, NiTiHf alloys can show low cyclic stability due to martensite reorientation stress, and plastic deformation of both the austenite and martensite phases can occur during transformation [33]. NiTiHf systems also tend to show wide hysteresis, low martensite finish temperature (M_f), problems with fabrication, and poor dimensional and thermal stability, all of which limit application potential [34].

To combat the potential downsides of NiTiHf, heat treatment procedures have been used extensively in literature strengthen the material while retaining toughness. A slightly Ni-rich composition assists in generating fine, nano-scale precipitates that strengthen the matrix in addition to tailoring transformation temperatures [6], [11], [33]–[35]. Evirgen et al. showed that short-term aging at 450 and 500°C created small intermetallics and decreased transformation temperatures, while aging at longer times and higher temperatures increased precipitate size and volume fraction and increased transformation temperatures.

Hardness testing has been used as a technique to predict HTSMA performance. Karaca et al. showed that Vickers hardness was an effective way to predict the "peak aging conditions" of $Ni_{50.3}Ti_{29.7}Hf_{20}$ [11]. Of the aging conditions tested, samples ages at 550°C for 3 hours had the highest hardness. Hardness is dependent on precipitate size and separation distance [6], and at 550°C 3h, NiTiHf has fine, densely spaced, coherent precipitates. Aging at higher temperatures results in increasing precipitate size and separation distance, leading to poor pseudoelastic behavior [11]. Just as hardness can effectively be used to predict pseudoelastic behavior, it may be a viable test for evaluating batch-to-batch variation in fatigue applications.

Isobaric heating-cooling (IHC) experiments on HTSMAs reveal many important characteristics for evaluating batch-to-batch variation. Karaca et. al. successfully used IHC data to distinguish between the performance of $Ni_{50.3}Ti_{29.7}Hf_{20}$ in three conditions: as-extruded, 550°C 3h, and 650°C 3h by comparing the compressive transformation

19

strains [11]. Similarly, transformation strain data could also be used to determine variation among batches of NiTiHf with the same target composition and transformation temperatures.

Studies in fatigue of $Ni_{50.3}Ti_{29.7}Hf_{20}$ specimens have been undertaken by Karakoc et. al., and it has been shown that upper cycle temperature (UCT) [36] and stress level [37] each have a clear influence on the fatigue life of HTSMAs. It is from the results of these studies in UCT and stress level that the question of batch-to-batch variation in HTSMAs has arisen.

Objectives

Additive Manufacturing of NiTi SMAs

While the majority of prior studies in additively manufactured NiTi have focused on studying compressive shape memory actuation or superelastic responses, tensile actuation of AM-fabricated NiTi has not been adequately addressed [30]. Characterizing tensile actuation is important since many applications of NiTi shape memory actuators operate under at least partial tension (such as bending) and the remnant porosity is one of the defects that may persist in AM parts and negatively affect the tensile properties, which may not have a notable effect on the properties under compression.

In this study, the viability of additively manufactured NiTi in tensile actuation is assessed. The transformations strains and irrecoverable strains of conventionally manufactured NiTi and two sets of additively manufactured NiTi, all with the same

20

initial composition, are compared to determine if AM NiTi can reasonably be used in tensile actuation applications.

NiTiHf High Temperature Shape Memory Alloys

NiTiHf has shown promise as a strong, fatigue-resistant, high work output shape memory alloy for use as tensile actuators in high-temperature environments. Recent studies [36], [37] in fatigue of NiTiHf in tension have revealed that different batches of NiTiHf produced under the same conditions, with the same target composition, but at different times, have shown differences in transformation temperatures and fatigue life at the same upper cycle temperature and stress level. The underlying microstructural and thermodynamic factors that could contribute to these differences in thermo-mechanical properties will be explored in this study.

Just as transformation strain data has been used to differentiate between sets of NiTiHf with different heat treatments [38] (and therefore, different transformation temperatures), transformation strain values determined through isobaric heating-cooling experiments could also be used to determine variation among batches of NiTiHf with the same transformation temperatures. Additionally, a series of monotonic tension experiments across a range of temperatures will help generate a stress-temperature phase diagram, which can reveal thermodynamic differences between NiTiHf batches.

CHAPTER II

EXPERIMENTAL PROCEDURES[2]

Material Processing

Laser Powder Bed Fusion of Nickel-Titanium

Conventionally manufactured (CM) $Ni_{50.9}Ti_{49.1}$ (at%) was originally obtained from SAES-Getters as a 1.5" diameter rod in hot-rolled condition. This Ni-rich NiTi composition was selected since Ni-rich side of the stoichiometry allows the control of transformation temperatures through the control of precipitates upon heat treatments. Some of this NiTi rod was used to fabricate dog-bone shaped miniature tension samples with a gage length of 8 mm, 1.0 mm thickness, and gage section width of 3.0 mm prepared with wire electric discharge machining (EDM), as shown in Figure 8. Flat squares with dimensions of 3 mm $\times$ 3 mm $\times$ 1 mm were cut using electrical discharge machining (EDM) for Differential Scanning Calorimetry (DSC). The tension and DSC specimens were prepared in order to compare shape memory properties between the AM and the conventionally manufactured samples.
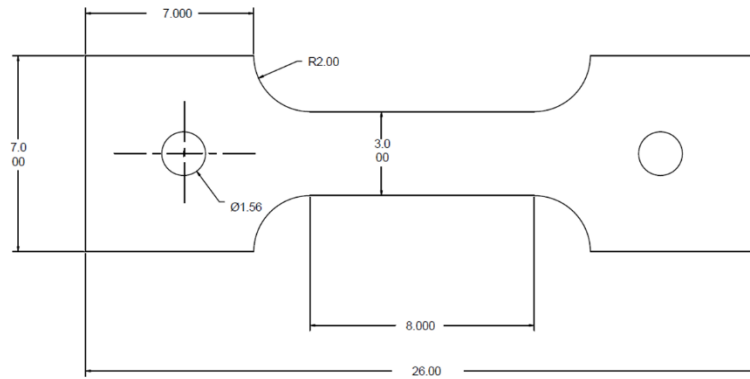
Figure 8. Schematic of a dogbone tensile specimen

The rest of the $Ni_{50.9}Ti$ rod was previously used to produce NiTi powder using gas atomization by Nanoval GmbH (d_{50} = 18.5 µm). Rectangular blocks with dimensions of 4 mm×8 mm×30 mm were fabricated on a 3D Systems ProX DMP 100 L-PBF AM system. Two sets of samples were produced. For both sets, the laser power, scanning speed, and layer thickness were kept constant at 50W, 80 mm/s, and 30 µm, respectively. These parameters were earlier shown to result in samples free of macro porosity and macro cracks [21]. Sample Set 1 (referred to as AM120) was fabricated with 120 µm hatch spacing, while Sample Set 2 (referred to as AM35) was fabricated with 35 µm hatch spacing. Hatch spacing refers to the distance between two adjacent passes of the laser beam within the same layer, and was chosen as the primary variable in this study because it was reported in previous work that it has a significant effect on transformation temperatures [21], [39]. The laser scanning pattern was alternated between perpendicular directions every other layer during printing. The effects of these

parameters on the shape memory / functional properties of a NiTi SMA under tension were first reported in this study [40].
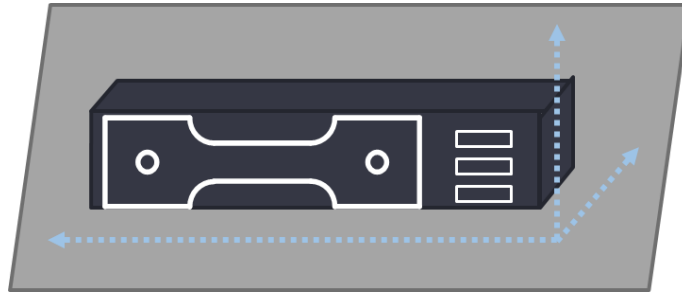
Figure 9. Tension and DSC specimen locations from L-PBF blocks

Tension and DSC specimens of the same dimensions as the CM material were cut from these blocks with Wire EDM to eliminate surface effects (Figure 9). Additionally, specimens cut from a $Ni_{49.7}Ti_{50.3}$ alloy (acquired from ATI in hot-rolled form) were similarly prepared as controls.

Induction-Melted Nickel Titanium Hafnium

Elemental Ni, Ti, and Hf (99.98%, 99.95% and 99.9% in purity, respectively) were used to fabricate a $Ni_{50.3}Ti_{29.7}Hf_{20}$ (at.%) alloy, which was induction melted in a graphite crucible and cast into a 1.25" diameter copper mold, which was homogenized at 1050°C for 72 hours in vacuum, and then extruded in a single pass at 900°C into a mild steel can, with area reduction ratios of 1.85:1, 3.7:1 (303 Series), and 6:1 (200, 301, and 500 Series), shown in Table 1. This condition is referred to as "as-extruded" or "as-

received" (ASR) throughout the paper. Composition measurements (Table 2) of the as-extruded material were made using ICP-AES on each batch of NiTiHf after extrusion.

Table 1. Extrusion ratios of multiple batches of NiTiHf

Series	Can OD (in)	NiTiHf OD (in)	NiTiHf (in^2)	Area Reduction (%) (initial / final area)
200	0.81	0.51	0.204	601%
301	0.81	0.51	0.204	601%
303	0.75	0.65	0.332	370%
500	0.81	0.51	0.204	601%

Table 2. Elemental compositions of multiple batches of NiTiHf

Series		Ni	Ti	Hf	Zr		C	N	O
200	*at%*	50.78	29.32	19.20	0.69	*wt%*	0.013	0.002	0.042
301/303	*at%*	50.76	29.57	19.43	0.24	*wt%*	0.005	0.002	0.036
500	*at%*	50.81	29.25	19.67	0.27	*wt%*	0.004	0.000	0.020

Flat squares with dimensions of 3 mm × 3 mm × 1mm were cut using electrical discharge machining (EDM) for DSC and hardness. These specimens were wrapped in tantalum foil and sealed in quartz tubes under vacuum of 1 x 10^{-5} torr and filled with argon. The specimens were then be heat treated in a Lindberg Blue M box furnace and quenched in water.

Dog-bone shaped miniature tension samples with a gage length of 8 mm, 0.8-1.5 mm thickness, and gage section width of 3.0 mm were prepared with wire EDM. These samples were then heat treated in air in a Lindberg Blue M box furnace at temperature of either 475°C or 550°C for three hours and air-cooled.

Differential Scanning Calorimetry

A TA Instruments Q2000 DSC instrument was used to measure the transformation temperatures of both the AM NiTi and NiTiHf. Flat squares with dimensions of 3 mm $\times$ 3 mm$\times$ 1 mm were prepared using EDM. The specimens underwent three DSC cycles at a heating/cooling rate of 10 °C/min, either from -100°C to 100°C or from -50°C to 150°C for AM NiTi, or from 50 °C to 300 °C for NiTiHf. Transformation temperatures were determined from the second-cycle DSC data (to eliminate first cycle effects) using the tangent line intercept method and TA Universal Analysis software.

Compositional Analysis

Local compositional analysis was conducted on some AM and CM NiTi DSC samples using Wavelength Dispersive Spectroscopy (WDS) in a Cameca SXFive Scanning Electron Microscope. Ten measurements were taken from each sample, and all samples were measured in the same session under the same beam conditions to minimize bias error between samples.

Stress-Temperature Phase Diagrams

Dogbone shaped miniature tension samples with a gage length of 8 mm were cut using EDM from both the conventionally manufactured NiTi samples and the AM-fabricated blocks. For the AM samples, the tension axis was perpendicular to the build direction and oriented either parallel or perpendicular to the laser scanning direction. The specimens were cut at least 0.5 mm away from the surface of the as-built block to eliminate the effect of surface defects. Both the AM and conventional NiTi samples were thermally cycled from approximately -50°C to 150°C under constant tensile stress levels in an MTS servohydraulic testing system, and the applied stress was increased incrementally after each heating-cooling cycle up to 500 MPa. For the AM NiTi samples, the heating-cooling experiment were repeated on three separate specimens to ensure reproducibility.

Dog-bone shaped miniature tension specimens (Figure 8) with thickness of 1.5 mm were cut using wire EDM from each batch of NiTiHf. Samples from each batch were thermally cycled in isobaric heating-cooling tests from approximately 50 °C to 300 °C under constant tensile stress levels of 50, 100, 150, 200, 300, 400, and 500 MPa in an MTS servohydraulic testing system. Applied force was measured with a load cell and strain was measured with an MTS high-temperature extensometer that had a gage length of 12 mm. The tension grips were heated through Joule heating and cooled via liquid nitrogen flowing through copper tubing. Temperature control was achieved through a

PID-capable Eurotherm controller with a precision of +/- 1°C. Transformation temperatures at each stress level were extracted from this data.

Similarly, dogbone shaped miniature tension specimens with thickness of 0.8 mm were also cut using wire EDM from each batch of NiTiHf. These specimens were heated to temperatures ranging from 25°C (M_s - 120°C) to 450°C (A_f + 275°C), and after stabilizing at a particular temperature, were strained monotonically in tension until failure. Stress-strain curves were generated for each batch of NiTiHf at each temperature, and the relevant values of interest (martensite reorientation stress, austenite yield stress, failure stress) were recorded and plotted in a stress-temperature phase diagram.

Vickers Hardness

Vickers hardness of AM NiTi and NiTiHf specimens was measured using a LECO LM300AT microhardness tester with a load of 300 kgf at room temperature. Ten measurements were taken at evenly distributed points along a 3 mm x 3 mm specimen. The specimen, which was previously used for DSC measurements, was mounted in epoxy and polished with SiC paper and diamond solution to the 1 μm level.

CHAPTER III

TENSILE ACTUATION RESPONSE OF ADDITIVELY MANUFACTURED NICKEL-TITANIUM SHAPE MEMORY ALLOYS[3]

Transformation Temperatures

Differential Scanning Calorimetry (DSC) experiments allowed for the measurement of transformation temperatures both before and after additive manufacturing. The portion of the stock $Ni_{50.9}Ti$ material that did not undergo gas atomization was analyzed under two conditions: as-received and aged at 450°C for 1.5 hours. The 450°C 1.5h heat treatment increased transformation temperatures and accentuated the sharpened the transformation peaks, indicating that the material had been homogenized during the heat treatment. These observations led to the conclusion that the $Ni_{50.9}Ti$ material had been optimized for a specific application and was used as the standard to which additively manufactured materials were compared.

---

[3] Part of the content reported in this chapter is reprinted with permission from "Tensile actuation response of additively manufactured nickel-titanium shape memory alloys," by J. Sam et. al., 2018. Scr. Mater., vol. 146, pp. 164–168, Copyright 2018 by Elsevier [40]
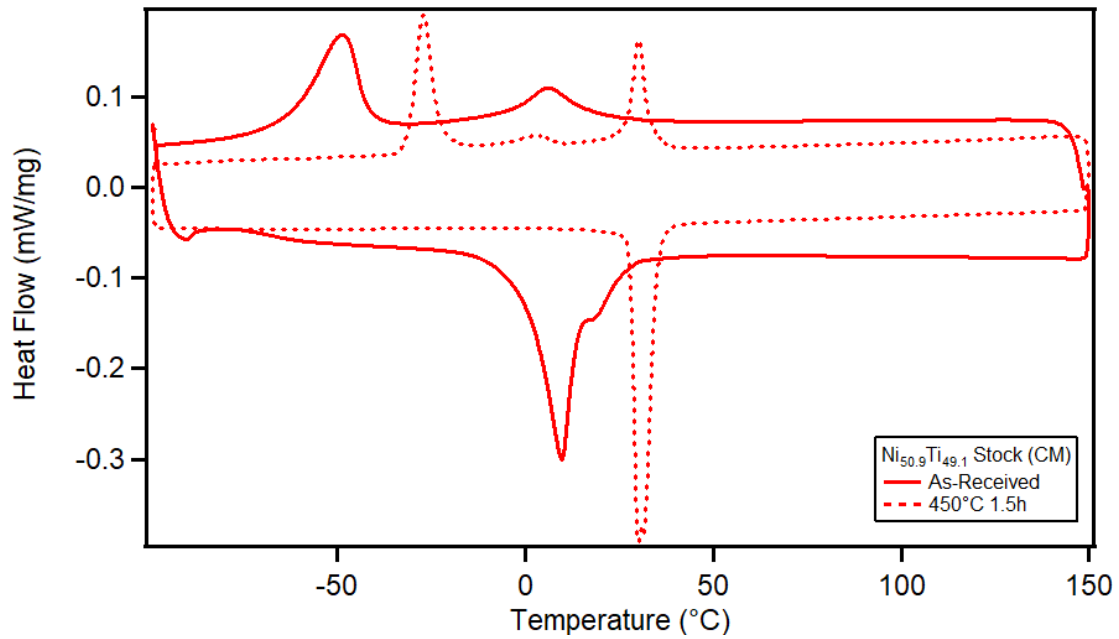
Figure 10. DSC curves of conventionally manufactured $Ni_{50.9}Ti$ stock

The DSC results of the additively manufactured $Ni_{50.9}Ti$ were analyzed to measure transformation temperatures. $Ni_{50.9}Ti$ AM120 (50 W laser power, 80 mm/s scan speed, 30 µm layer thickness, 120 µm hatch distance) was assessed for consistency in transformation temperatures in different locations across the build after printing (Figure 11). The AM120 build showed consistency between samples in different locations, and in general, showed a broad transformation with no visible R-phase.
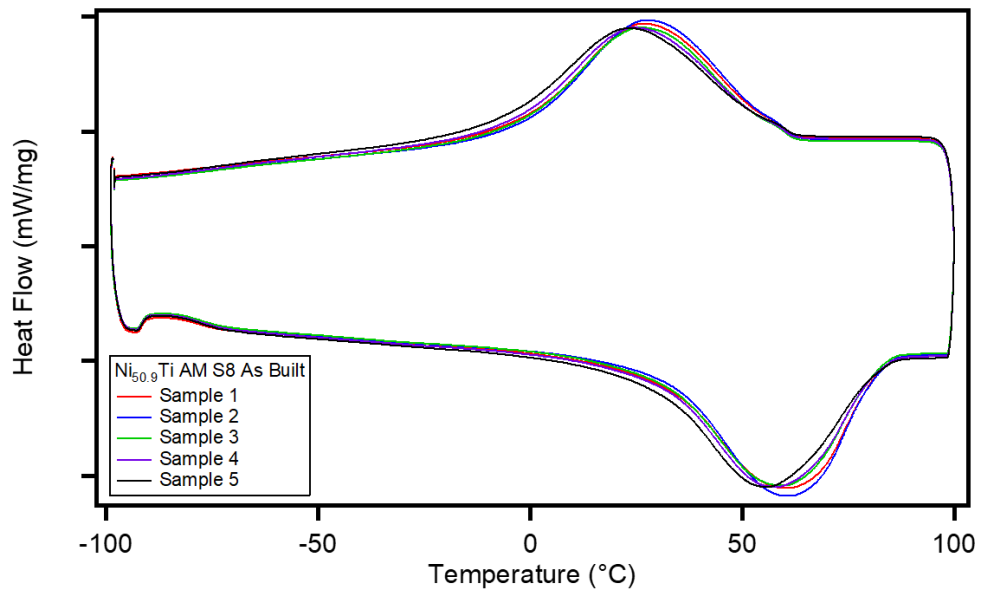
Figure 11. DSC curves of multiple AM120 samples

Similarly, $Ni_{50.9}Ti$ AM35 (50 W laser power, 80 mm/s scan speed, 30 μm layer thickness, 35 µm hatch distance) showed stable, repeatable transformation (Figure 12). In contrast to AM120, AM35 showed a much narrower, two-stage transformation. In general, narrow transformations are preferable to broad ones because the transformation temperatures are easier to designate for actuator applications.
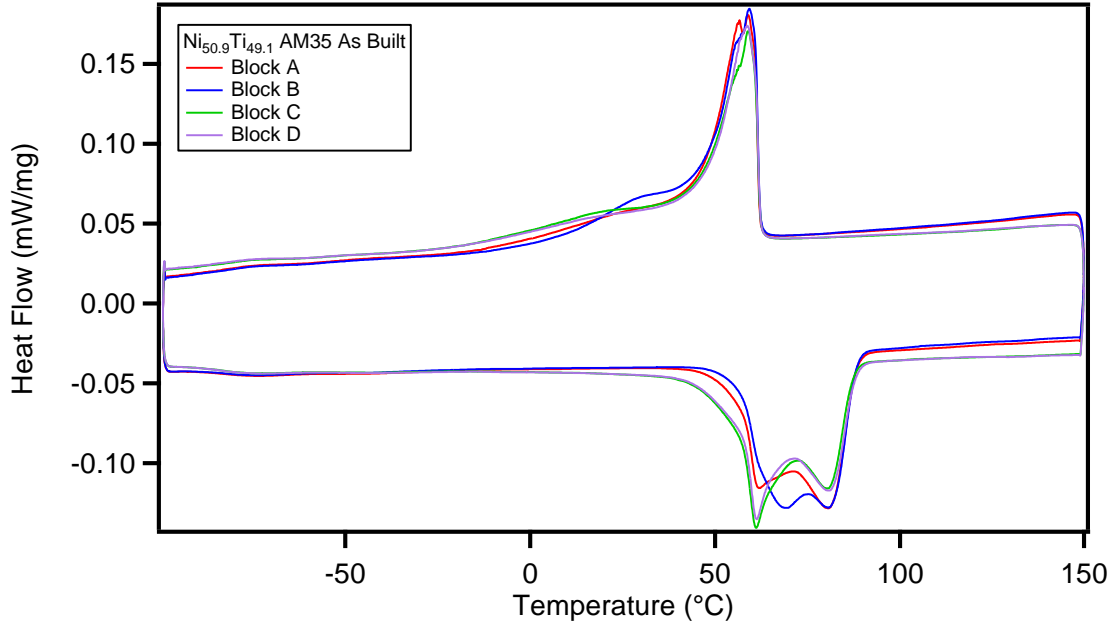
Figure 12. DSC curves of multiple AM35 samples

The effect of SHT on the DSC results of AM NiTi is reported in Figure 13 and Table 3. SHT of the AM120 samples at 900°C for 1 hour did not result in changes of the martensite (24°C) or austenite (56°C) peak temperatures but reduced the width of the peaks (M_s-M_f or A_s-A_f), indicating that the solution heat-treatment made the samples more homogeneous or eliminated AM-induced defects. This suggests that the as-fabricated samples have local inhomogeneity in their composition or microstructure. The as-fabricated samples also show shallower transformation peaks (or lower transformation enthalpy) than solution treated cases (Figure 13), which indicates the presence of microstructural features that resist phase transformation.

32
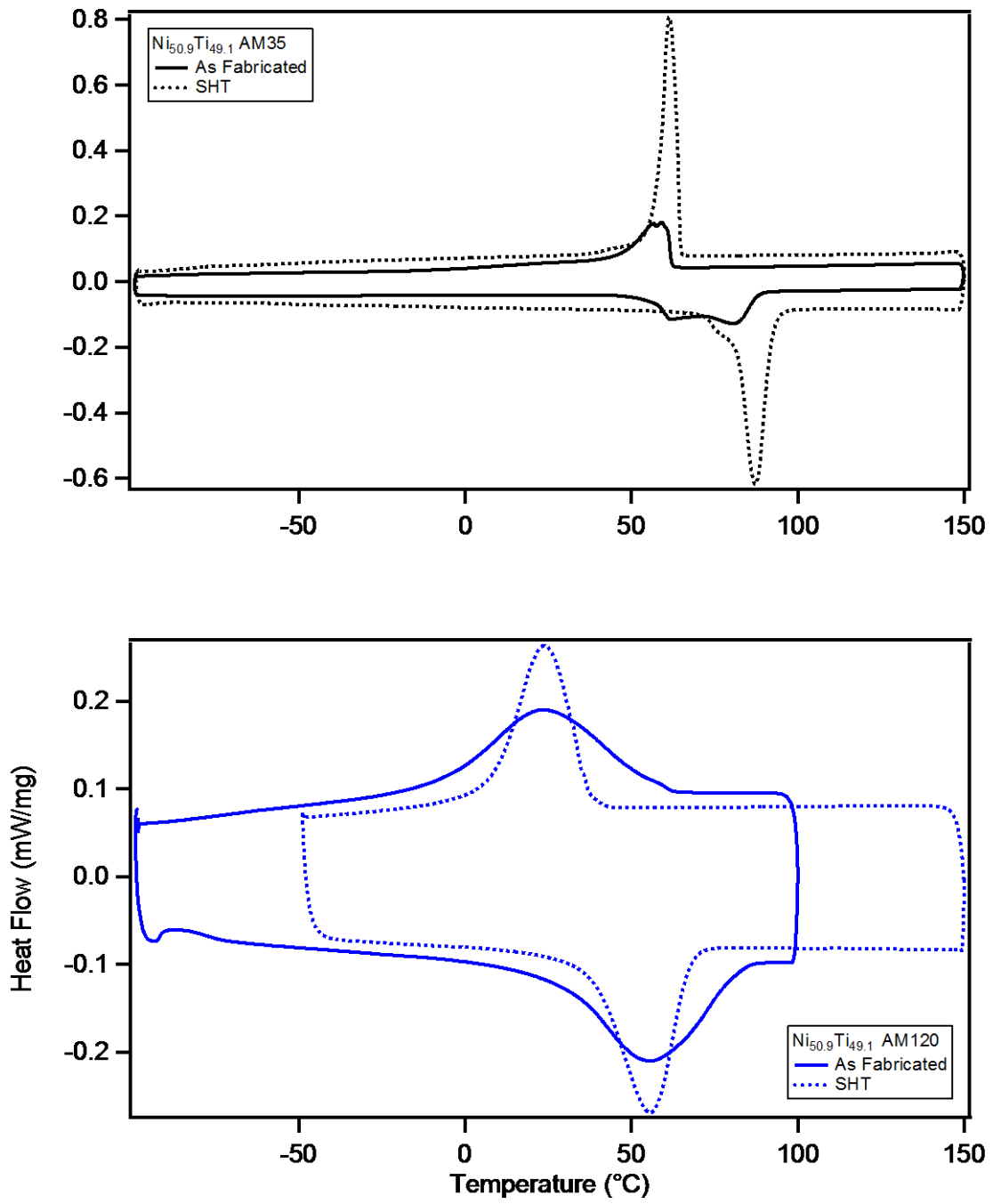
Figure 13. DSC curves of as-fabricated and solution heat-treated AM35 and AM120

Table 3. Transformation temperatures for conventionally manufactured and additively manufactured $Ni_{50.9}Ti_{49.1}$

	M_f (°C)	M_s (°C)	A_s (°C)	A_f (°C)	M_p (°C)	A_p (°C)	Ms-Mf (°C)	Af-As (°C)
Ni50.9Ti Stock	-70	-52	-22	-8	-58	-14	18	14
Ni50.9Ti Stock SHT	no transformation							
Ni50.9Ti AM35	47	62	56	88	59	81	15	32
Ni50.9Ti AM35 SHT	56	65	80	93	61	87	9	12
Ni50.9Ti AM120	-2	57	33	82	24	56	60	49
Ni50.9Ti AM120 SHT	8	37	39	67	24	56	28	29

Figure 14 compares the DSC results for AM samples (AM35 and AM120) in the solution heat-treated (SHT) case with the DSC results for conventionally manufactured (CM) $Ni_{50.9}Ti$ in the As-Received (AR) condition. The corresponding transformation temperatures are presented in Table 3. The transformation temperatures of the as-fabricated NiTi AM samples are considerably higher than that of the conventionally manufactured alloy. The AM35 samples show higher transformation temperatures than AM120 samples in both the as-fabricated and SHT conditions. Since NiTi transformation temperatures are inversely proportional to nickel content, these two observations indicate that L-PBF AM causes significant nickel loss, more so in AM35 than AM120. This nickel loss has been reported in additive manufacturing literature and is attributed to nickel evaporation during L-PBF process since nickel has a lower boiling point than titanium [26].
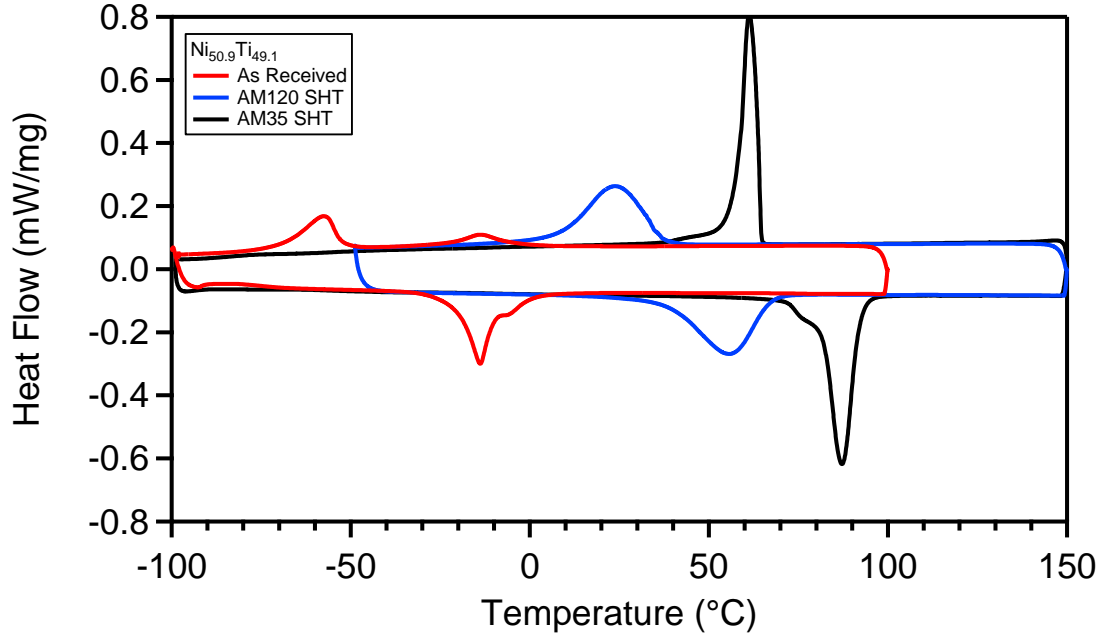
Figure 14. DSC curves for as-received $Ni_{50.9}Ti$, SHT AM35 and SHT AM120 $Ni_{50.9}Ti$

Compositional Analysis

The results of the Wavelength Diffraction Spectrometry (WDS) compositional analysis are shown in Table 4. The measurements of four samples after SHT are listed: conventionally fabricated $Ni_{50.9}Ti_{49.1}$ and $Ni_{49.7}Ti_{50.3}$ samples, and AM35 and AM120 samples fabricated in this study. The two conventionally manufactured samples were selected as a baseline; since their compositions are known, the measured compositions of the AM samples are compared to the baseline samples to eliminate the effect of systematic errors of the WDS. As seen in Table 4, there is a systematic error of approximately 0.8-0.9 at.% overestimation in titanium content and a corresponding 0.8-0.9 at.% underestimation in nickel content. Nevertheless, these results show that the

AM35 sample is heavily titanium rich (~52 at% Ti), and the AM120 sample is roughly

equiatomic (~50% Ti). This confirms that a large amount of nickel evaporation has

occurred during the fabrication process, and the loss is greater in the AM35 sample than

that in the AM120.

Table 4. Compositions of AM and CM NiTi specimens

	AM35	$Ni_{49.7}Ti_{50.3}$	AM120	$Ni_{50.9}Ti_{49.1}$
Nickel (at. %)	46.57	49.12	49.42	50.01
Titanium (at. %)	53.43	50.88	50.58	49.99

Mechanical Behavior

Room-temperature monotonic tension tests were conducted to generate stress-

strain data for each additively manufactured NiTi material and compare them to the

conventionally manufactured $Ni_{50.9}Ti$ material (Figure 15a). The CM $Ni_{50.9}Ti$ material

showed much greater ductility (30.6% strain) and yield stress (414 MPa), in comparison

to 3.4% strain and 134 MPa yield stress for AM35 and 7.1% strain and 107 MPa yield

stress for AM120.
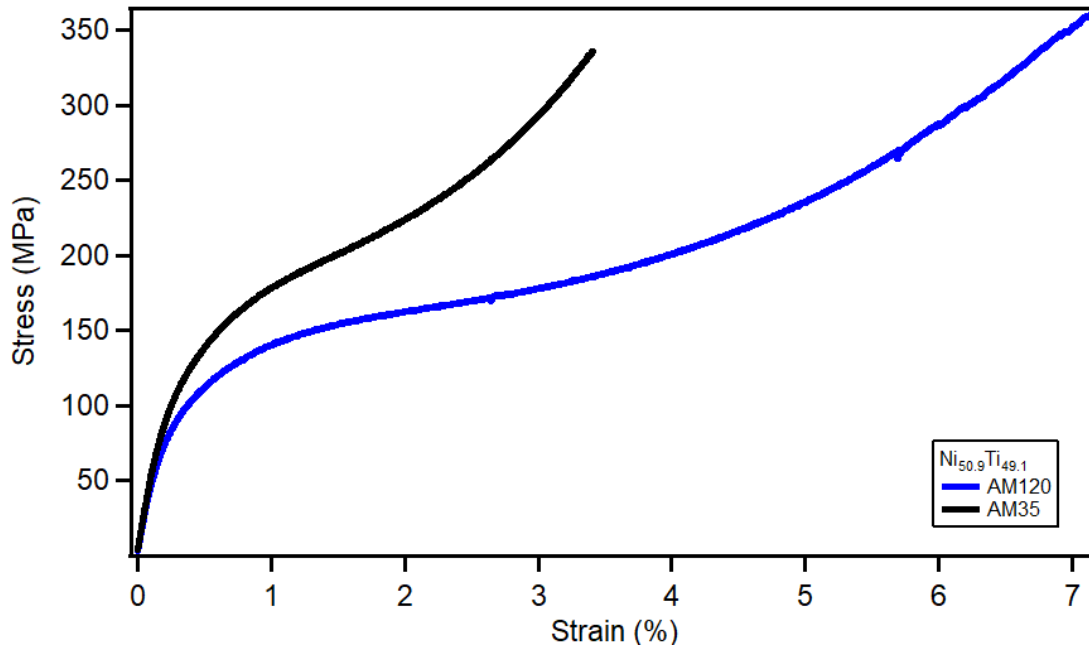
Figure 15. Stress-strain curves for NiTi AM120 and AM35

These results indicate that the mechanical properties of specimens printed with these AM parameters are significantly worse than the original material. During the printing process, the microstructure that is created lacks the strengthening mechanisms generated by precipitates and other microstructural features in the original material. Additionally, the ductility of the printed specimens is much lower, indicating that there might be small cracks in the printed specimens that propagate quickly under tension loading or non-metallic inclusions such as oxides or carbides.

The difference in mechanical properties between the two printed specimen sets is shown in Figure 15b. AM120 exhibits greater ductility, but lower yield stress than AM35. This may be due to a difference in dislocation density, precipitate size, and/or volume fraction.

Thermo-mechanical Behavior

The present study is among the first attempts in characterizing tensile actuation response of nickel-rich NiTi SMAs produced using L-PBF AM. In addition, it is demonstrated how shape memory characteristics such as transformation temperatures and actuation strain can be controlled through varying AM process parameters. The AM and conventionally fabricated samples were subjected to thermal cycles under constant tensile loads in order to characterize their shape memory actuation behavior and strain recovery (Figure 16 and Figure 17).
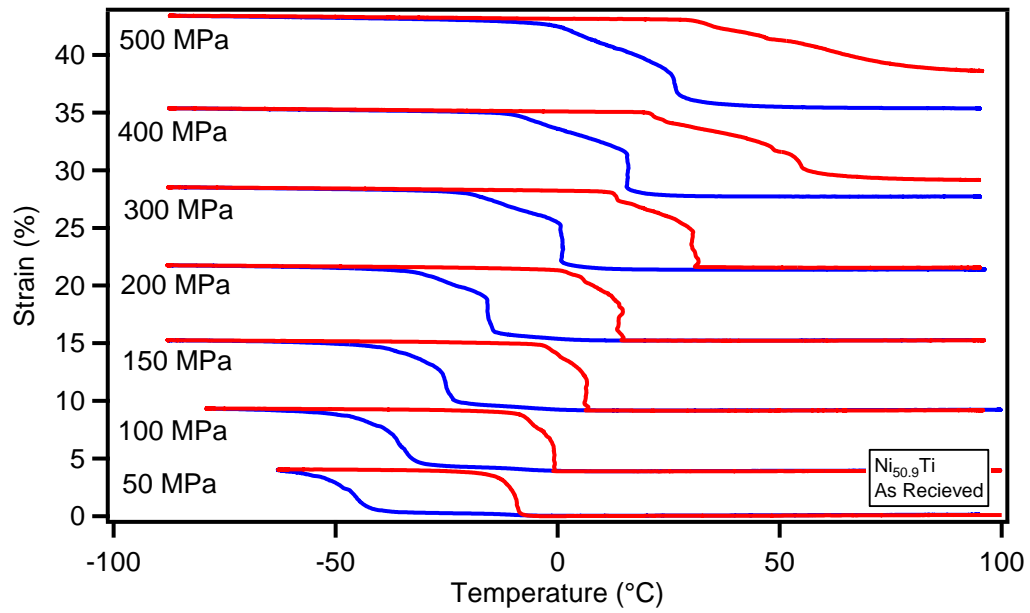
Figure 16. Isobaric heating-cooling results for conventionally manufactured $Ni_{50.9}Ti$
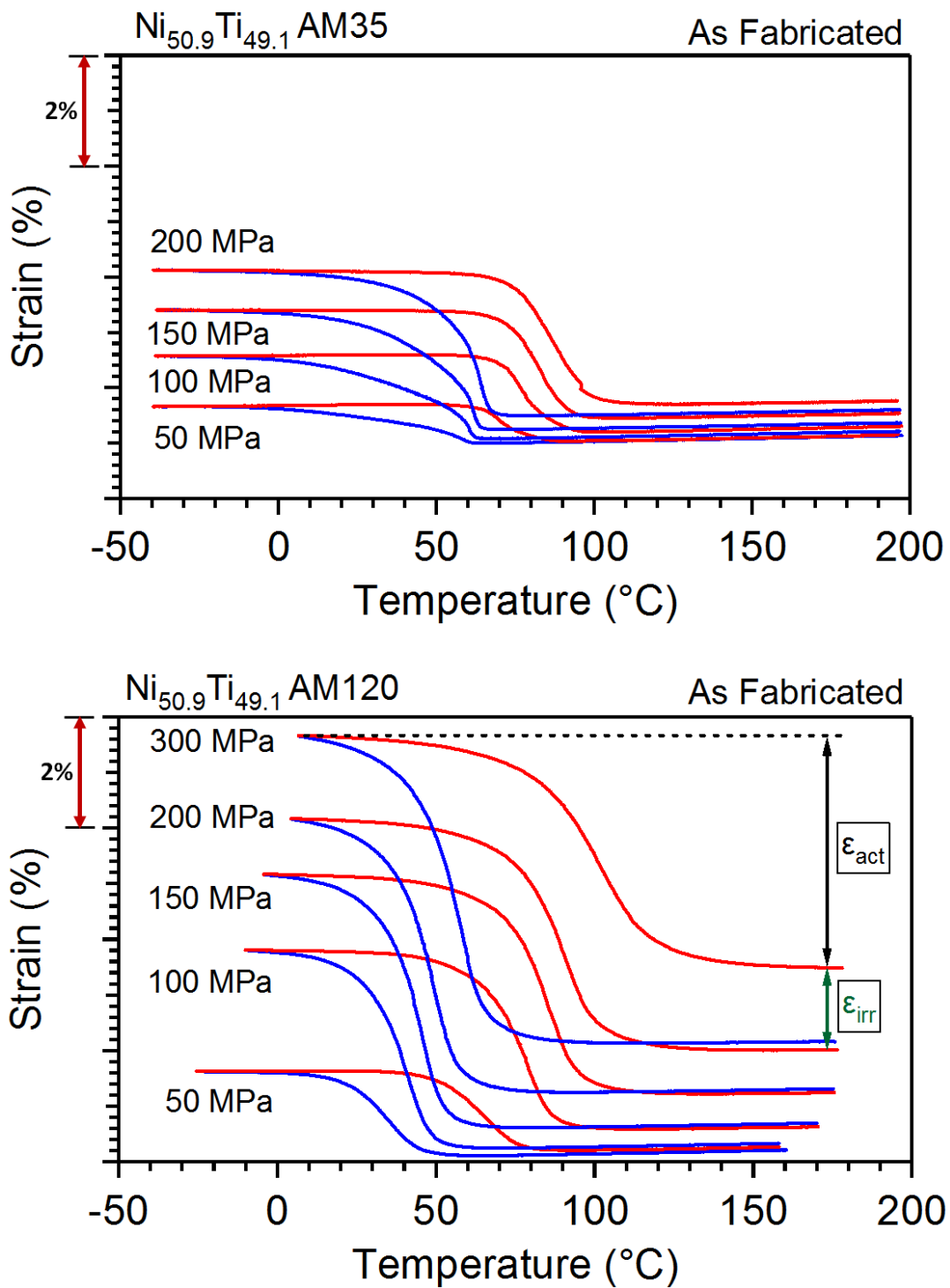
Figure 17. Isobaric heating-cooling results for AM NiTi (a) AM35 (b) AM120

The stress levels were increased in 50 MPa increments up to 200 MPa, and in 100 MPa increments above 200 MPa until the sample fractured or significant irrecoverable strain accumulated. Figure 18 shows representative results from the strain vs. temperature responses for each of the four cases tested. Three samples were tested for each condition. All AM120 samples failed below 400 MPa, while AM35 samples failed below 300 MPa. The actuation and irrecoverable strains were determined from the strain vs. temperature curves as shown in Figure 17c and a summary of these strains is presented as a function of applied stress in Figure 19.
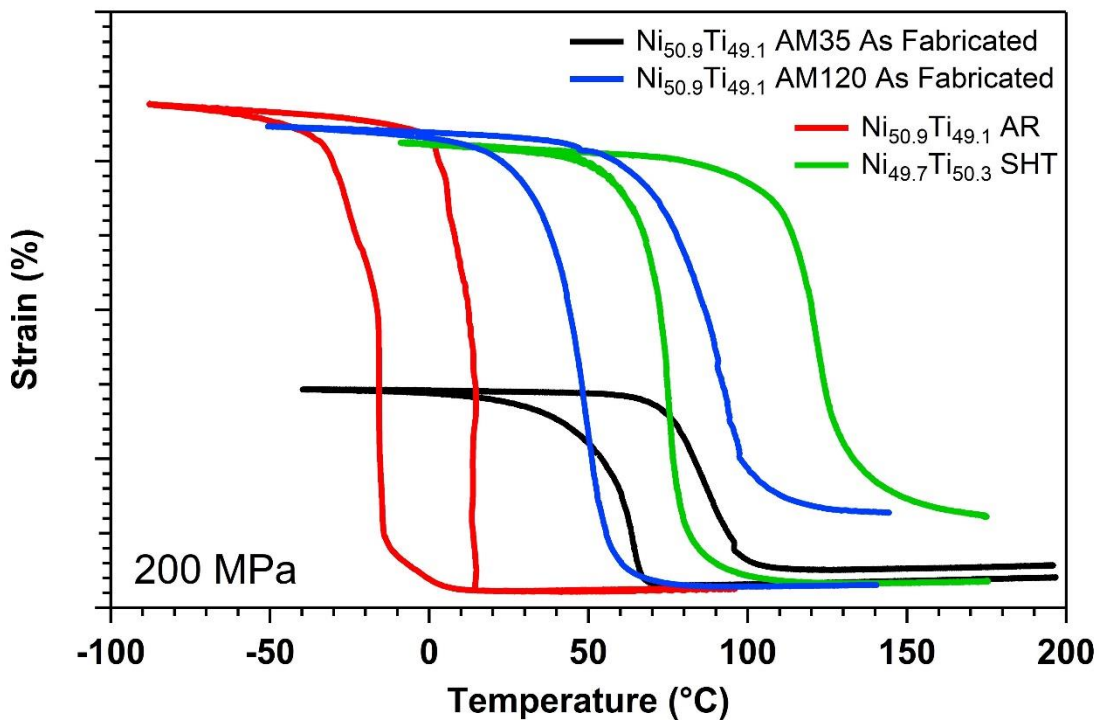
Figure 18. Comparison of isobaric heating-cooling results at 200 MPa for various NiTi compositions
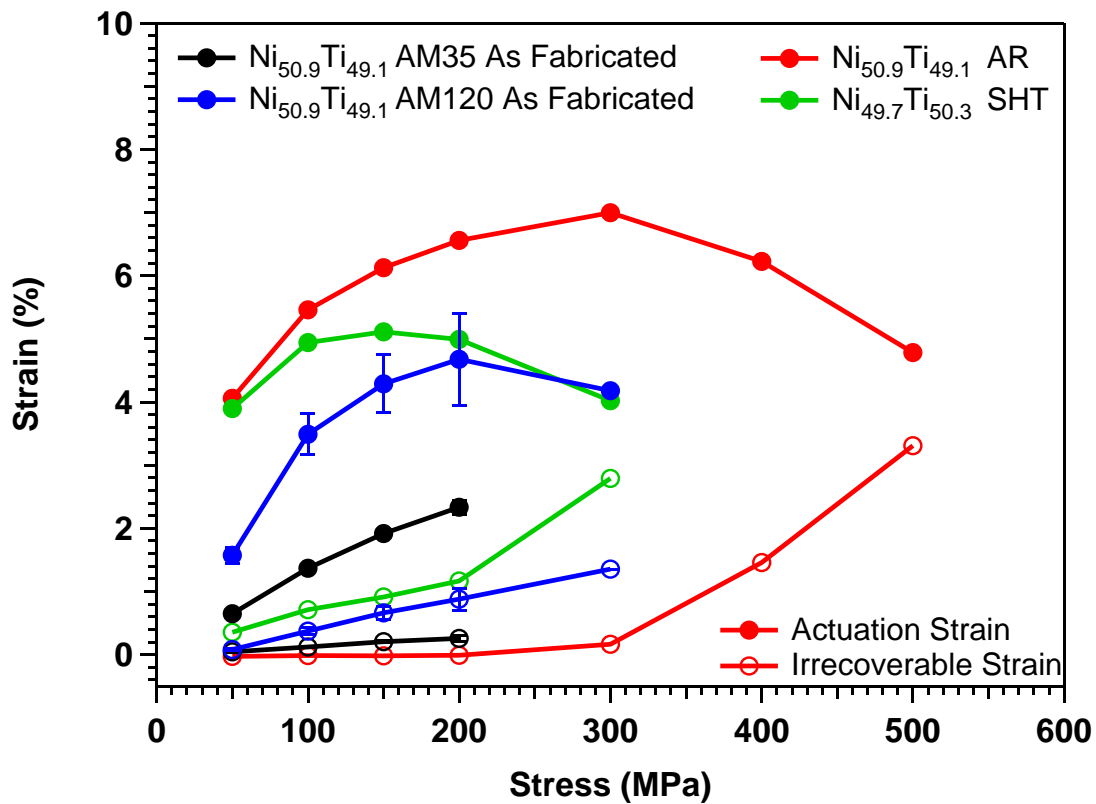
Figure 19. Actuation strain and irrecoverable strain for various NiTi compositions

The as-fabricated AM samples show significantly lower actuation strains and higher irrecoverable strains than the conventionally manufactured $Ni_{50.9}Ti_{49.1}$ material. However, this observation must be contextualized in two ways: first, it is important to note that the conventionally fabricated $Ni_{50.9}Ti_{49.1}$ material was received in the condition with an optimized heat treatment to maximize strengthening effects due to precipitation hardening. As seen in the DSC curve in Figure 10, the as-received $Ni_{50.9}Ti_{49.1}$ shows two distinct transformation peaks during cooling, the first of which corresponds to the B2 → R phase transformation which is expected in Ni-rich NiTi with Ni_4Ti_3 precipitates. On

42

the other hand, no additional post-fabrication heat treatment was performed on the AM NiTi samples. Second, based on the compositions measured using WDS shown in Table 4, both the AM35 and AM120 cases have experienced significant nickel loss during fabrication such that they have become equiatomic or titanium-rich. Nickel-rich precipitates such as Ni_4Ti_3 are not expected to form, and thus, a more appropriate comparison for these samples is the equiatomic NiTi SMA.

Indeed, the AM120 sample shows tensile actuation response comparable to that of solution treated equiatomic NiTi SMAs as shown in Figure 18 and Figure 19. The AM samples show slightly improved resistance against plastic deformation (i.e. lower irrecoverable strains) and lower actuation strains at lower stress levels – although the maximum actuation strains are similar. On the other hand, the AM35 sample shows significantly lower actuation and irrecoverable strain levels. For all cases, the AM35 sample fractured below 300 MPa, while the AM120 samples failed mostly below 400 MPa. Failure generally occurred during cooling near the M_f temperature. This is likely a result of build defects in the material such as porosity or non-metallic inclusions of carbides and oxides. Similar challenges have been reported in the AM fabrication of other metallic alloys such as Ti-6Al-4V [14], and porosity can be reduced through optimization of the processing parameters or employing a second laser pass within each layer [41]. Such techniques would likely be effective for NiTi SMAs as well.

Interestingly, the sample-to-sample variability in both the actuation strain and irrecoverable strain appear larger in the AM120 samples compared to the AM35 samples

(Figure 19). This agrees with previous work where the sample-to-sample variability in

transformation temperatures was also found to be larger in the AM120 samples [39],

indicating that the sample-to-sample variability in the transformation temperatures may

be a good indication for the sample-to-sample variability in the actuation properties of

the AM NiTi samples. The reason for such variability in the transformation temperatures

was shown to be the local microstructural variations in the samples because of the large

hatch distance and thus, different number of melting/heating cycles at different locations

of a given laser pass [18].

The reported tensile actuation response of the AM120 sample is comparable to

that of the compression actuation response in nickel-rich NiTi SMAs with similar

processing parameters [16]. However, the response of the AM35 sample is dramatically

different, and shows much more resistance to both phase transformation (lower actuation

strain) and dislocation plasticity (lower irrecoverable strain). In fact, the response of the

AM35 sample mimics the actuation response of significantly strengthened SMAs

through heavy precipitation hardening, for example in $Ni_{55}Ti_{45}$, or cold working or

severe plastic deformation [12], [42].

Based on the microstructural studies performed in our previous works on these

two fabrication conditions [21], [39], the grain size and second phase distributions are

not significantly different. However, the dislocation density in the AM120 sample

appeared to be higher than that in the AM35 sample (Figure 20). This evidence would

suggest that the AM120 sample should show greater resistance to deformation compared

to the AM35 sample, but the opposite was observed in the current work. A potential

explanation for this discrepancy was also reported previously [21], [39], where small (<2

nm) nano-precipitates were observed in the AM35 sample (Figure 20**Error! Reference**

source not found.c). It is not clear whether these precipitates are also present in the

AM120 sample, or at least present in comparable volume fractions. Because of their

size and the presence of larger precipitates of Ti_2Ni around 10-20 nm in size, the small

precipitates have been challenging to image and characterized and the subject of an

ongoing investigation.

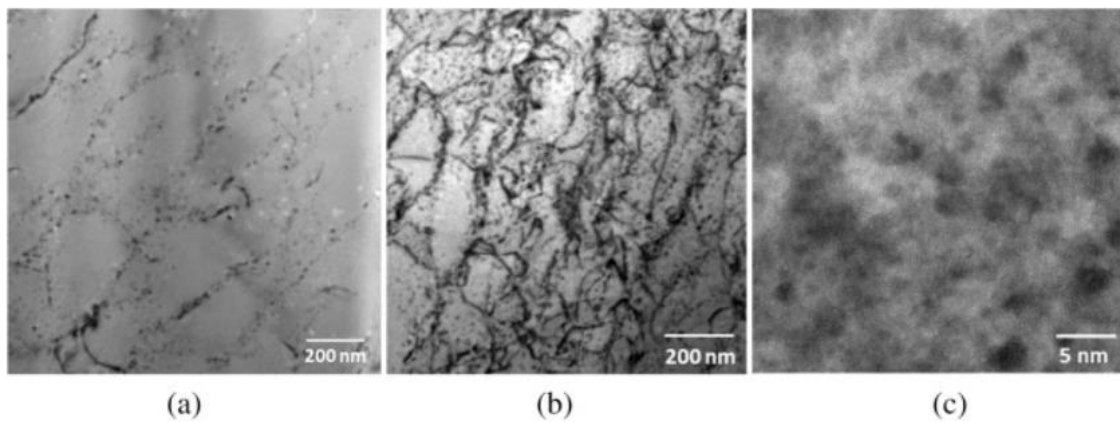(a)   (b)   (c)

Figure 20. Bright field TEM images of the AM fabricated NiTi samples: (a) AM35 sample and (b) AM120 sample showing the differences in the dislocation densities due to the different thermal histories. Specimens have been tilted to show maximum contrast of the dislocations. (c) Higher resolution image of the AM35 sample showing small < 2 nm precipitates. (reprinted from [40])

CHAPTER IV

BATCH-TO-BATCH VARIATION OF NITIHF HIGH-TEMPERATURE SMAS

Fatigue Results

The four batches of NiTiHf arrived in waves over the course of a few years, upon which they were tested in fatigue experiments. The "200" series was the baseline against which subsequent series were compared. The "301" and "303" series arrived together, with the additional variable of extrusion ratio (Table 1). The "500" series arrived last, and experiments testing the effect of upper cycle temperature [36] and applied stress [37] on fatigue results were performed on all four series. Each published work limited results to one series of material, in order to remove the effect of batch-to-batch variation.

In agreement with previously published literature, 550°C for 3 hours was chosen as the aging treatment for the 200 series. This heat treatment was selected because it led to the highest reversibility of martensitic transformation in comparison to other heat treatments. This is due to the coherent nano-precipitates that are formed during aging [11], [36], [43]. The "300" series (301 and 303) had significantly different transformation temperatures from the 200 series. Considering this, a different aging treatment was chosen for the 300 series (475°C 3h) to match the transformation temperatures of the 200 series. The 500 series material had the same transformation temperatures as the 200 series, so the aging treatment of 550°C 3h was used.

Over the course of this testing, batch-to-batch variation in fatigue life was observed between series on specimens tested under the same conditions of stress and

upper cycle temperature. The 301 series had the greatest number of cycles to failure by a wide margin, followed by the 500 series, the 200 series, and then the 303 series. On the other hand, the 200 and 500 series demonstrated excellent stability (lack of change in actuation strain over time), while the 301 and 303 series both showed instability, with actuation strain quickly depreciating and suppressing transformation. All four series had the same target composition ($Ni_{50.3}Ti_{29.7}Hf_{20}$) and 303 had an extrusion ratio of 3.7:1, while the other three series had extrusion ratios of 6:1 (Table 1).
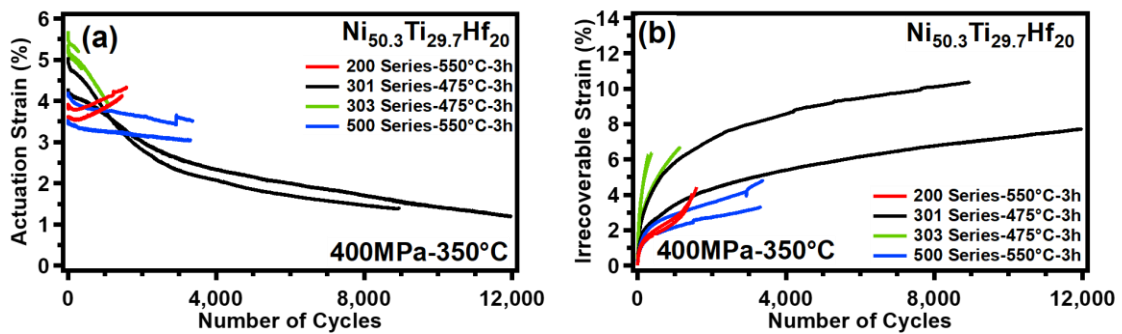
Figure 21. Fatigue results of NiTiHf. (a) Actuation strain (%) vs. number of cycles (b) Irrecoverable strain (%) vs. number of cycles

An HTSMA that has strong potential to be used as a material for a linear actuator would be characterized by a combination of high actuation strain, stable actuation strain, and many cycles to failure. To quantify these parameters, a new parameter called "actuation potential" (AP) was developed, according to the following equation:

$$AP = \frac{N_f}{\varepsilon_i - \varepsilon_f}$$

Where N_f is the number of cycles to failure, ε_i is the initial actuation strain, and ε_f is the final actuation strain.

Table 5. Fatigue data of NiTiHf

Series	Specimen	Stress (MPa)	Heat Treatment	Avg Strain (%)	# of Cycles	Work Output	Initial Strain (%)	Final Strain (%)	Irr. Strain (%)	Instability (ε_i-ε_f) (%)	Actuation Potential
200	**207-10**	400	550°C-3h	3.9	1589	15.56	3.68	4.25	4.2	0.57	27.9
	209-24	400	550°C-3h	3.74	1468	14.98	3.61	4.12	4.11	0.51	28.8
301	**301-24**	400	475°C-3h	2.29	8952	9.15	5.06	1.39	9.15	3.67	24.4
	301-82	400	475°C-3h	2.19	11962	8.74	4.3	1.2	7.71	3.1	38.6
303	**303-21**	400	475°C-3h	4.6	1135	18.35	5.36	3.88	6.67	1.48	7.7
	303-22	400	475°C-3h	4.96	374	19.85	5.32	4.77	6.37	0.55	6.8
500	**500-71**	400	550°C-3h	3.2	3307	12.8	3.56	3.04	3.31	0.52	63.6
	500-80	400	550°C-3h	3.49	3496	13.96	3.75	3.36	3.6	0.39	89.6

Based on these calculations, it can be estimated that the 500 series shows the best promise in actuator applications, while the 200 and 301 series would have moderate performance and the 303 series would show poor performance. The results of the following sections were interpreted in light of these conclusions regarding estimated actuator performance.

Transformation Temperatures

As batches of NiTiHf were obtained for use in fatigue experiments, DSC experiments were conducted to measure transformation temperatures and hysteresis (A_f - M_s). As shown in Table 6 and Figure 22a, the transformation temperatures of the 301 and 303 series in the as-received condition were much higher than that of the 200 and 500 series material. Solution heat treatment (at 900°C for one hour) was performed on all batches to restore the material to a precipitate-free state. This procedure was successful in the 200 series, as noted by the sharper transformation peak for the solution heat-treated case, indicating the removal of precipitates that impede shape memory transformation (Figure 22b). Unfortunately, though solution heat treatment sharpened the peak of the DSC curves of the 301 and 303 series, it did not solve the discrepancy between the transformation temperatures of the 301/303 series and that of the 200/500 series.

Table 6. Transformation temperatures of multiple batches of NiTiHf

		Series	Mf (°C)	Ms (°C)	As (°C)	Af (°C)	Af-Ms (°C)
As Received		**200**	63	101	103	133	32
		301	121	145	159	177	32
		303	122	144	161	174	30
		500	70	86	106	123	37
Solution Heat Treated (900°C 1h)		**200**	76	95	110	128	33
		301	139	158	172	185	26
		303	145	166	187	199	33
		500	83	95	122	131	36
Aged	**550°C 3h**	**200**	123	154	151	177	23
	475°C 3h	**301**	132	150	162	177	27
	475°C 3h	**303**	142	159	171	182	24
	550°C 3h	**500**	131	147	161	175	28

Since the heat treatment of the 300 series had to be adjusted by 75°C to match the transformation temperatures of the 200 series in its peak-aged condition, it can be reasonably concluded that the 300 series has a higher nickel content than the 200 and 500 series. Although this was not evident in the ICP results from the supplier (Table 2), there is significant evidence from literature that nickel content has a strong effect on transformation temperatures.
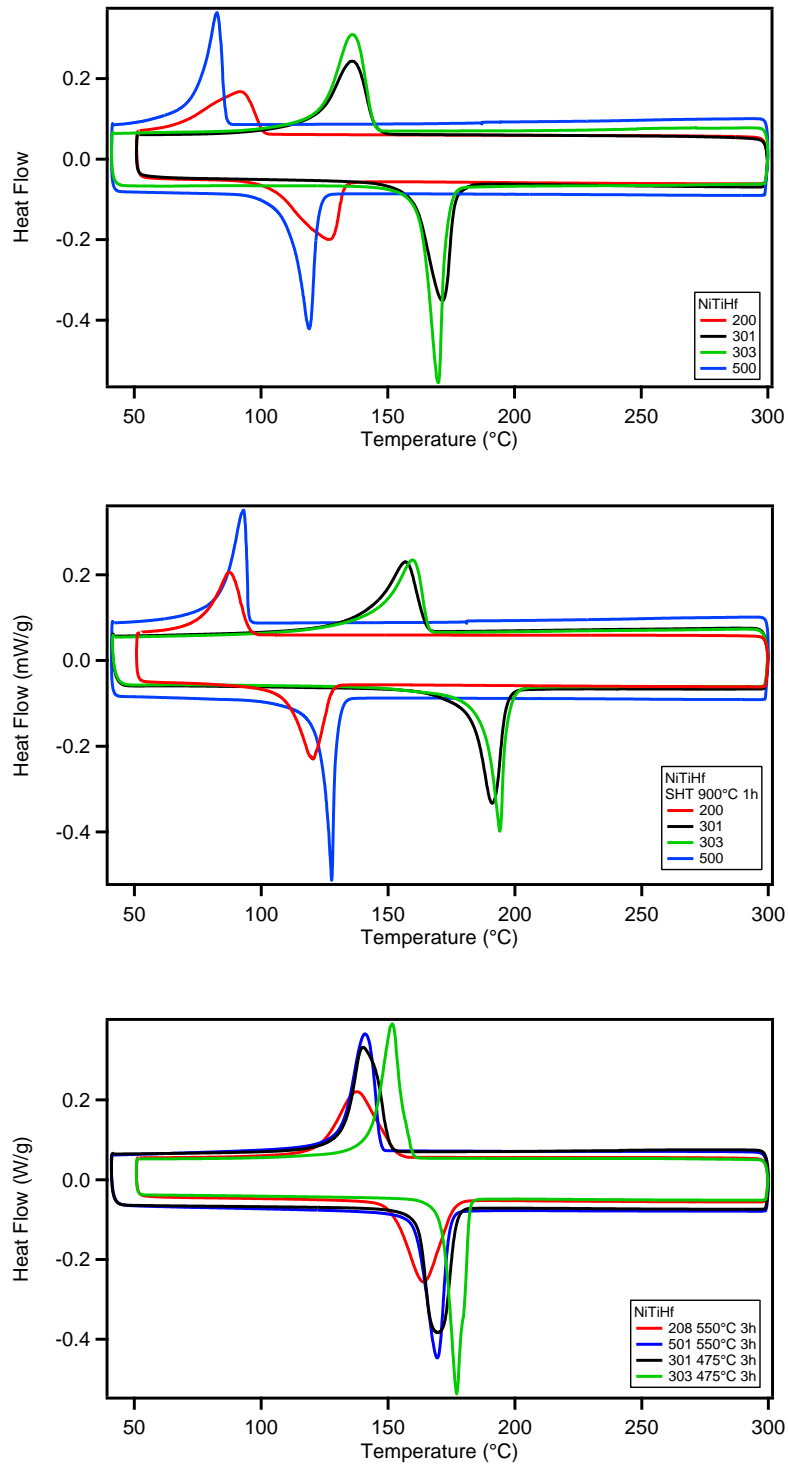
Figure 22. DSC results of multiple batches of NiTiHf
(a) As-Received condition (b) Solution heat-treated condition (c) Peak-aged condition

Precipitate Size

Precipitate size was observed in three NiTiHf batches (200, 301, and 500) through TEM (Figure 23). It was observed that samples of NiTiHf the 200 and 500 series both had precipitates of similar size and shape, while the 301 series had much smaller precipitates. The 200 and 500 series both had a high fatigue stability, while the 301 series had low stability, quickly depreciating in actuation strain from cycle to cycle. Since full actuation strain did not occur in later cycles, the 301 series was able to have a longer fatigue life than any other batch of NiTiHf, indicating that functional fatigue (because of martensitic transformation) took longer to occur. Because of this correlation, it can be concluded that batches of NiTiHf with larger precipitates (on the order of the precipitates in 200 and 500) have greater cyclic stability, while batches with smaller precipitates may have lower cyclic stability and show depreciation of actuation strain over the course of fatigue experiments. This hypothesis make sense because small precipitates are typically more coherent in the NiTiHf matrix, which may explain the greater influence of small precipitates on impeding full transformation. This smaller particle size may be a function of the lower nickel content in the 301 series (as indicated by DSC).
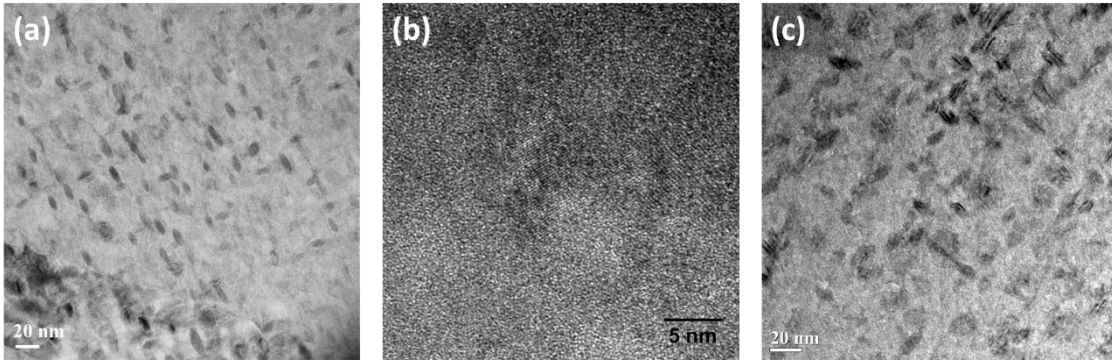
Figure 23. TEM images showing precipitates in NiTiHf
(a) 200 series (b) 301 series (c) 500 series (adapted from Omer Karakoc, unpublished)

Carbide Content

SEM images were taken of specimens from the 200, 301, 303, and 500 series. In these images, carbides (most likely titanium carbide) were observed in all four batches. Based on the SEM images for each series, an analysis of carbide area fraction was performed (Figure 24). These results show a distinct difference between the carbide content of the 200, 300, and 500 series, which is correlated to the carbon content found in the elemental analysis (Table 2). This correlation was plotted in Figure 25, and had a correlation coefficient of 0.9428.
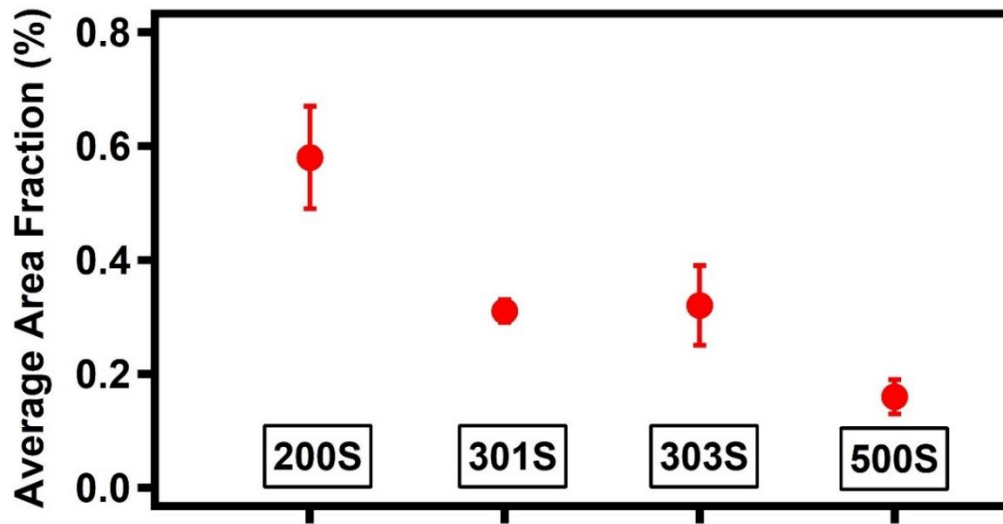
Figure 24. Carbide area fraction comparison for multiple batches of NiTiHf
(adapted from Omer Karakoc, unpublished)

Figure 25. (a) Carbide area fraction as a function of carbon content, (b) actuation potential as a function of carbide content

The actuation potential was also plotted as a function of carbide content, and a

slight correlation was found when using a logarithmic regression ($r^2 = 0.6941$). Since the

carbides are not coherent in the NiTiHf matrix, they may not necessarily impede

55

martensitic transformation (functional fatigue) but rather may function as stress

concentrators, and the presence of carbides may lead to greater crack formation and

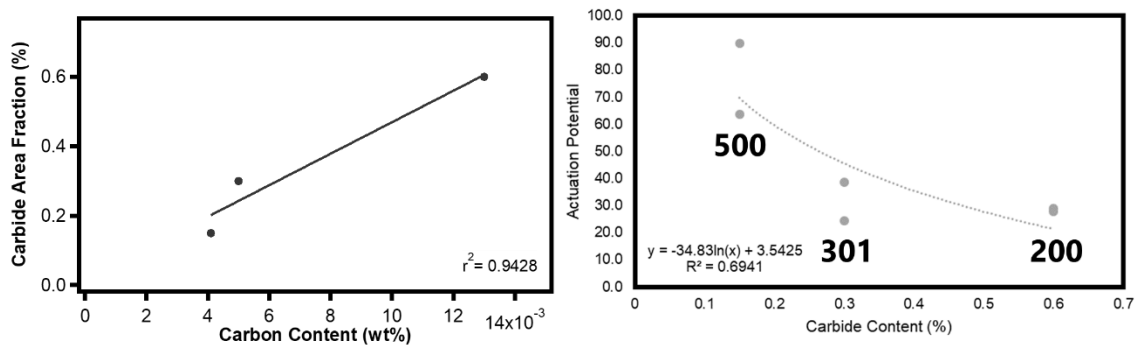propagation, shortening fatigue life (structural fatigue). In a comparison between the 200

and 500 series, which have similar levels of stability (Table 5), the increased presence of

carbides in the 200 series has a direct correlation with the shorter fatigue life of the 200

series. This increased carbide formation may be a function of slight differences in the

manufacturing process, which involves the use of a graphite crucible.

Vickers Hardness

Vickers hardness measurements were proposed to predict actuation potential as a

function of heat treatment temperature (Figure 26), in the spirit of experiments such as

those conducted by Karaca et. al. [11]. Unfortunately, no clear trends could be observed

within the data obtained. A more thorough study could lead to observation of a

correlation between hardness value at a particular temperature and fatigue life, stability,

or actuation potential.
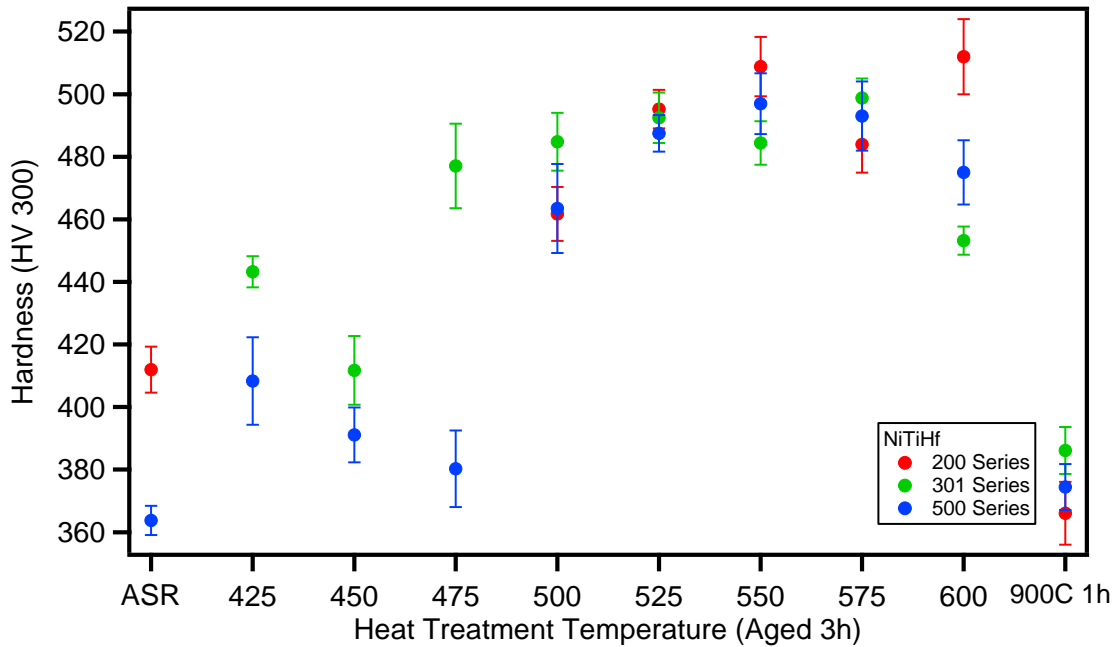
Figure 26. Hardness results of multiple batches of NiTiHf

Mechanical Behavior

Stress-strain curves were generated using monotonic tension tests to failure for each batch across a range of temperatures. The purpose of these experiments was to assess whether simple tension tests could be used as a screening method to predict thermo-mechanical actuation fatigue behavior. Most test temperatures led to mixed results (Appendix) but tests at 25°C (Figure 27) and at 250°C (Figure 28) showed differences in stress-strain behavior that could be attributed to microstructural factors that correspond to fatigue behavior.

Figure 27. Stress vs. strain of NiTiHf at 25°C

Figure 28. Stress vs. strain of NiTiHf at 250°C

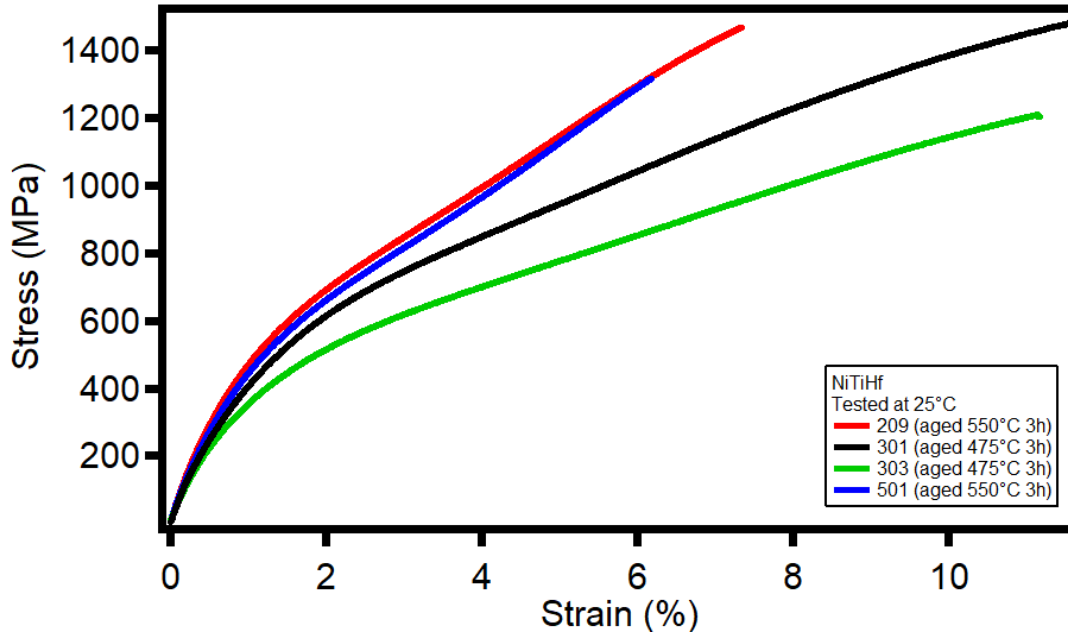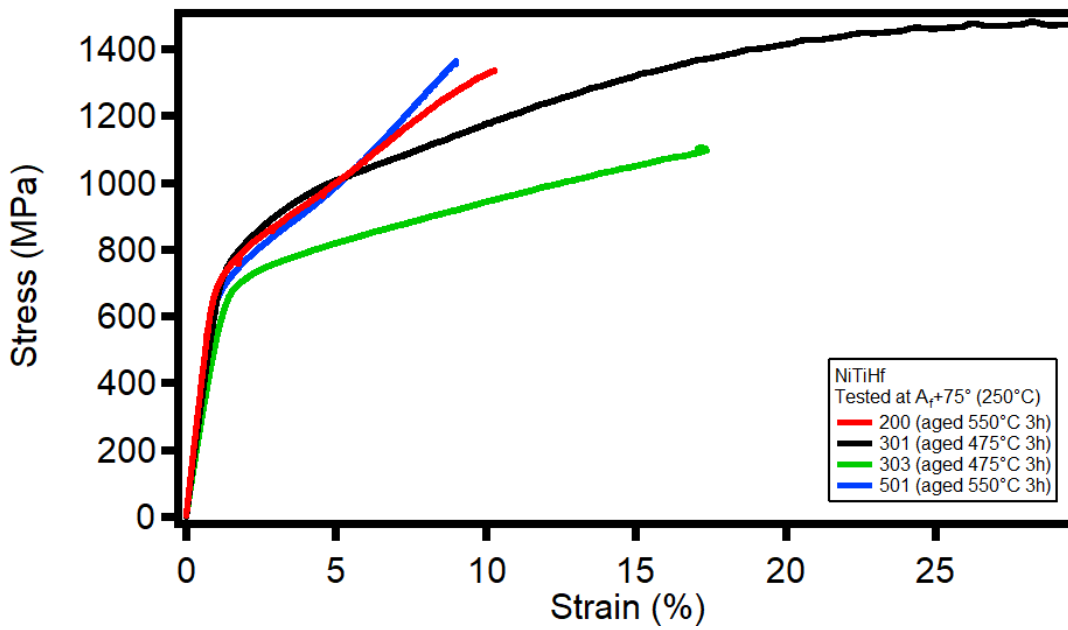At room temperature (25°C), shown in Figure 27, the 200 and 500 series had higher martensite reorientation stress and greater strain hardening than the 301 and 303 series, indicating greater strength (perhaps due to the higher titanium content). In contrast, 301 and 303 showed greater ductility at this temperature.

At 250°C (75°C above the austenite finish temperature), the stress strain curves (Figure 28) showed a similar pattern as the room temperature curves (strain hardening in 200 and 500 and ductility in 301 and 303). The higher nickel content of the 300 series (as indicated by DSC) could potentially cause an increase in plasticity, which explains the greater ductility of the 301 and 303 series across virtually all temperatures.

Considering these results, room temperature tension testing and tension testing above A_f could be used as screening methods to identify mechanical differences (most likely a function of composition) that correspond to fatigue performance; namely, the higher nickel content/ductility of 301 and 303 correspond to high instability/depreciation of actuation strain as a function of number of cycles.

Thermo-mechanical Behavior

Isobaric heating-cooling experiments were performed to assess the transformation profiles, actuation strain, and irrecoverable strain of each batch of NiTiHf. A comparison of the heating-cooling cycles at all stress levels for each batch is shown in Figure 29. Visual inspection of these curves leads to the qualitative observation of greater transformation hysteresis (area between martensite and austenite curves) for the 301 and 303 series as compared the 200 and 500 series.
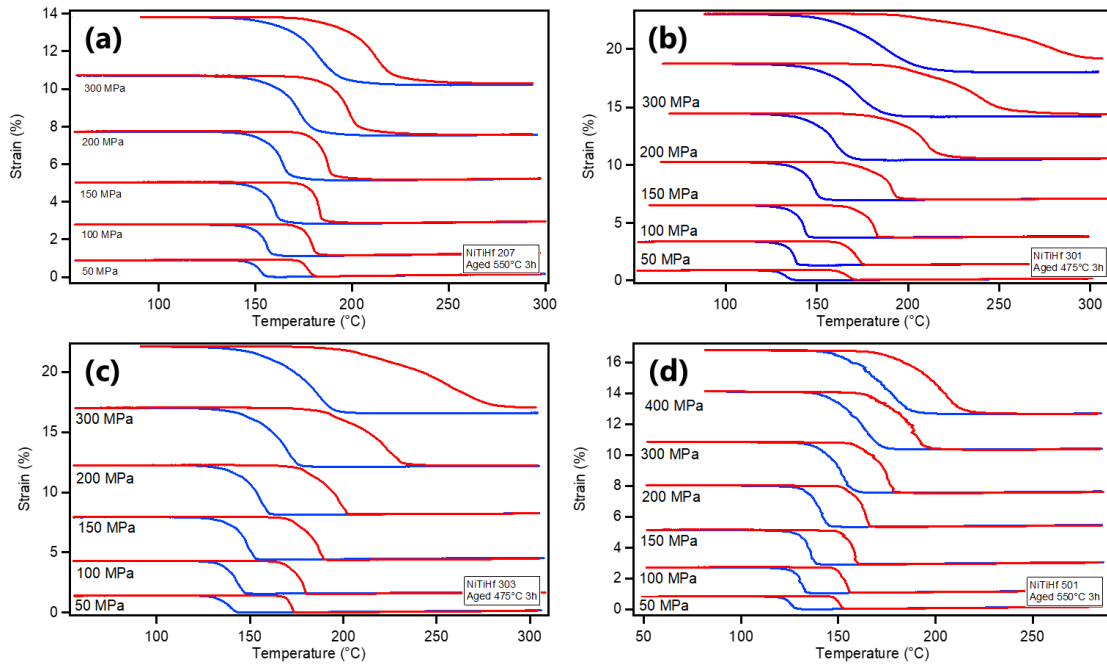
Figure 29. Isobaric heating-cooling curves for NiTiHf
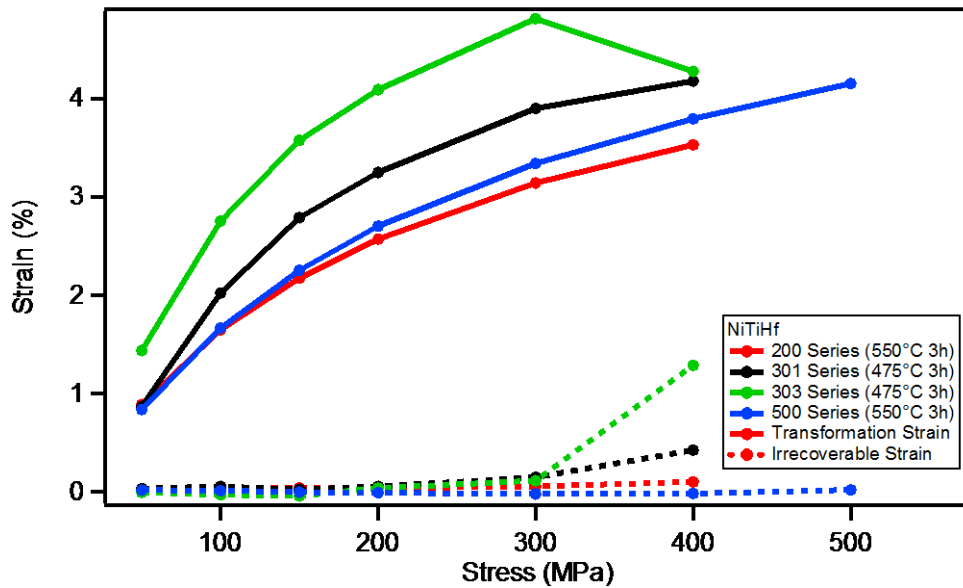(a) 200 series (b) 301 series (c) 303 series (d) 500 series

Figure 30. Strain vs. stress of NiTiHf

60

A quantitative analysis of transformation strain and irrecoverable strain for each batch is shown in Figure 30. Here, it is shown that the 301 and 303 series show more transformation strain over one cycle than 200 and 500, under the same loading conditions. However, the irrecoverable strain of 301 and 303 is considerably higher (this effect is pronounced at the 400 MPa level). These two measurements may help explain the depreciation of actuation strain during the fatigue experiments of 301 and 303. On each actuation cycle, the 301 and 303 series, due to the small, coherent precipitates contained within (Figure 23), lacks reversibility in transformation strain. This leads to an accumulation of non-transforming regions in the matrix, effectively reducing the potential for actuation strain in future cycles. The 200 and 500 series have larger precipitates, which do not disrupt reverse transformation as much, leading to greater reversibility and lower irrecoverable strain.

Stress-Temperature Phase Diagrams

The transformation temperatures from the isobaric heating-cooling experiments, in addition to the Martensite Reorientation and Austenite Yield points from the stress-strain curves, were combined to developed stress-temperature phase diagrams for each series (Figure 31). The goal of these diagrams was to observe differences between batches of NiTiHf in thermodynamic relations, such as Clausius Clapeyron slope (M_s slope), austenite yield slope (A_y slope), or difference between stress at M_d and stress and M_s (σ_{Md} - σ_{Ms}).
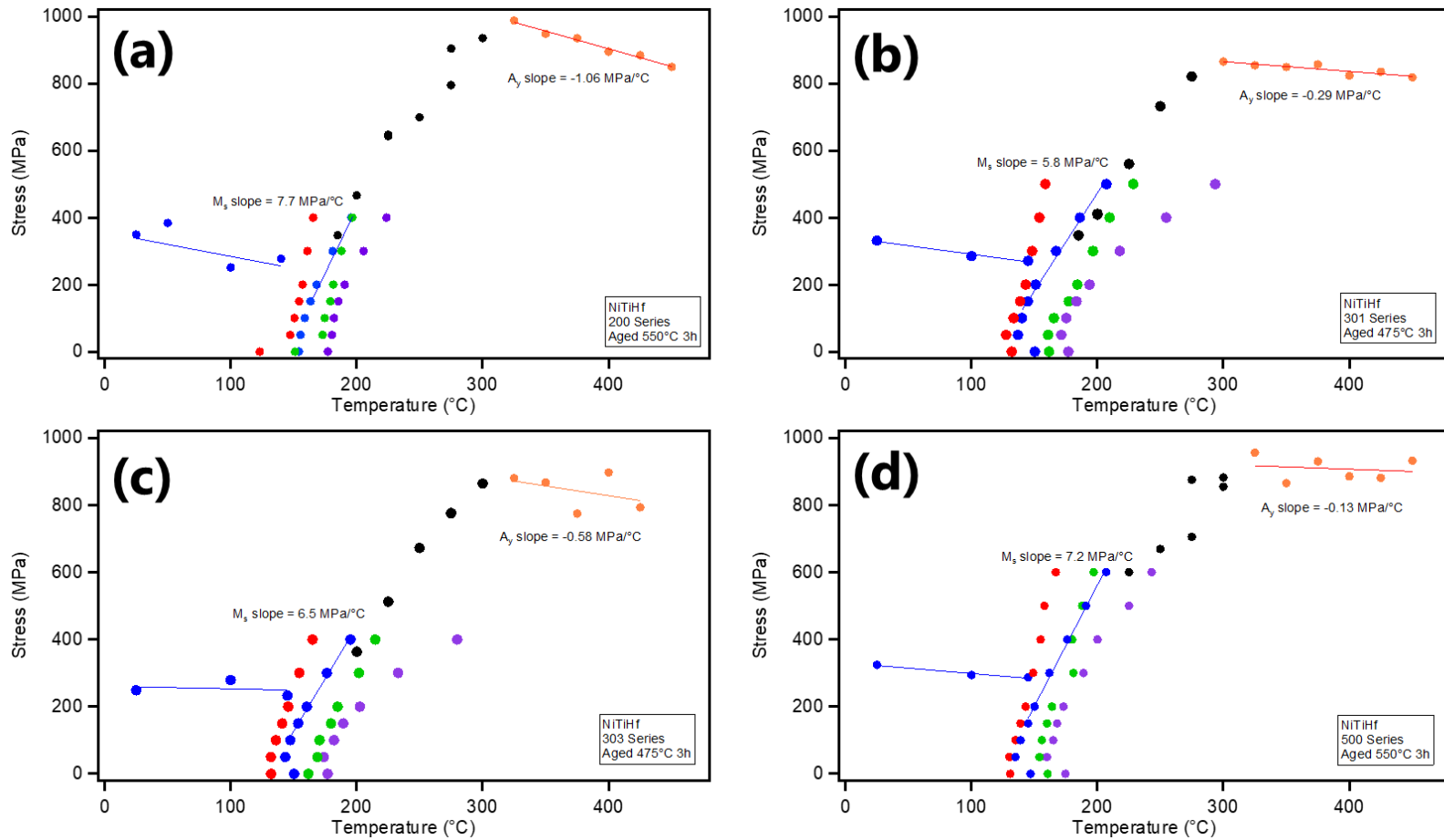
Figure 31. Stress-temperature phase diagrams for NiTiHf. (a) 200 Series (b) 301 Series (c) 303 Series (d) 500 Series

Karaca et. al. reported a Clausius-Clapeyron (M_s) slope of 7.5 MPa/°C for polycrystalline $Ni_{50.3}Ti_{29.7}Hf_{20}$ aged at 550°C for three hours [11]. The measured M_s (martensite start temperature) slopes for the 200, 301, 303, and 500 series were 7.7, 5.8, 6.5, and 7.2 MPa/°C, respectively. The values for the 200 and 500 series (which have similar properties to other $Ni_{50.3}Ti_{29.7}Hf_{20}$ specimens from literature) are like that of Karaca et. al., while the 301 and 303 series (which, due to smaller precipitates and high nickel content) have smaller M_s slopes.

The measured A_y (austenite yield) slopes for the 200, 301, 303, and 500 series were -1.06, -0.29, -0.58, and -0.13 MPa/°C, respectively. These values do not correlate with any other observable differences between the batches.

The difference between stress at M_d and stress and M_s (σ_{Md} - σ_{Ms}) for the 200, 301, 303, and 500 series were 711, 594, 647, 669 MPa respectively. This parameter did not correlate well with any parameters for fatigue performance.

CHAPTER V

SUMMARY AND CONCLUSIONS

Tensile Actuation of Additively Manufactured NiTi SMAs[4]

Summary

The ability of additive manufacturing to control dimensions, microstructure, and chemistry makes it an extremely precise and versatile manufacturing method. Additive manufacturing can be used successfully to manufacture shape memory alloys, but there are many challenges in matching the mechanical properties of additively manufactured parts to their conventionally manufactured counterparts. However, more research needs to be done to fully understand the effects of additive manufacturing techniques and bring additively manufactured SMAs to their full potential.

Tensile actuation responses of L-PBF-processed AM NiTi SMAs have been studied, and the actuation responses in the as-processed condition are comparable to that of a precipitate-free conventionally fabricated NiTi of near-equiatomic composition. The actuation strain levels and reversibility of the as-processed AM NiTi SMA are inferior to that of the conventionally fabricated and aged Ni-rich NiTi SMAs. Significant nickel loss was observed in all AM NiTi samples. Although measurable tensile actuation was observed under relatively high stress levels, the AM NiTi is nevertheless observed to be

---

somewhat brittle. Furthermore, it is demonstrated that by changing L-PBF processing parameters, both the transformation temperatures and the tensile actuation responses can be modified and potentially controlled. These differences are believed to be caused by composition changes from preferential nickel evaporation and microstructural variations caused by differences in the thermal history during processing.

Future Work

It is critical to conduct experiments on a larger number of samples to characterize the variability of both the actuation and mechanical response of the L-PBF-processed alloys for qualification and certification for mission critical applications. Additional work should be performed on either optimization of processing parameters or post-fabrication processing to improve the fracture resistance of the material.

Batch to Batch Variation of NiTiHf High Temperature SMAs

Summary

A diverse selection of experiments were conducted to seek factors that influence fatigue performance of high-temperature shape memory alloys and whether certain experiments could be used as screening tools for predicting fatigue performance.

Room temperature and Af+75°C (250°C) monotonic tension tests (Figure 27, Figure 28) can potentially screen for low strength or high ductility, which is a sign of actuation degradation in fatigue. This phenomenon is an examples of functional fatigue, a consequence of cyclic martensitic transformation.

Smaller precipitates (such as those in the 301 series, observed in Figure 23) can cause actuation strain to degrade with repeated cycling, because these precipitates are more coherent in the matrix and inhibit transformation. This is another example of functional fatigue.

High carbide levels (indirectly measured with elemental analysis in Table 2 and directly measured by calculation area fraction from TEM results in Figure 24) lead to short fatigue life because they act as stress concentrators, initiating small cracks that lead to failure. This is an example of structural fatigue and can be screened by measuring carbon content immediately after extrusion.

Future Work

Several open questions remain regarding batch-to-batch variation in $Ni_{50.3}Ti_{29.7}Hf_{20.}$ The primary open question regards the irregular DSC results of the 301 and 303 series. Although it is proposed that there in higher nickel in these batches than 200 and 500, this hypothesis was not proven with elemental analysis. Perhaps there is an unknown mechanism or microstructural feature causing the 300 series to behave as if it had higher nickel. Nevertheless, this variation in transformation temperatures in the as-received condition, if not ameliorated, can lead to non-optimal heat treatments and reduced fatigue performance.

The reasons behind the poor performance of 303 in comparison to 301 are not fully understood. Although there was an intentional difference in extrusion ratio during manufacturing, the microstructural differences between the two batches are not fully

understood. It is hypothesized that this difference is in grain size or texture but attempts to measure these parameters did not achieve dependable results. Perhaps in-situ (high temperature) observation of average relative grain sizes can help understand the effect of extrusion ratio on microstructure.

Hardness was proposed as a simple screening method for predicting fatigue performance, but the data collected (Figure 26) did not lead to clear conclusions. Perhaps a more thorough study of hardness as a function of heat treatment and composition can be used to predict actuation fatigue properties.

REFERENCES

[1]   J. M. Jani, M. Leary, A. Subic, and M. A. Gibson, "A review of shape memory alloy research, applications and opportunities," *Mater. Des.*, vol. 56, pp. 1078–1113, 2014.

[2]   L. C. Chang and T. A. Read, "Plastic Deformation and Diffusionless Phase Changes in Metals - The Gold-Cadmium Beta-Phase," *Trans. Am. Inst. Min. Metall. Eng.*, 1951.

[3]   W. J. Buehler, J. V. Gilfrich, and R. C. Wiley, "Effect of Low-Temperature Phase Changes on the Mechanical Properties of Alloys near Composition TiNi," *J. Appl. Phys.*, vol. 34, no. 5, pp. 1475–1477, 1963.

[4]   W. J. Buehler, "WOL Oral History Supplement," 2006.

[5]   S. Dadbakhsh, M. Speirs, J. Van Humbeeck, and J.-P. Kruth, "Laser additive manufacturing of bulk and porous shape-memory NiTi alloys: From processes to potential biomedical applications," *MRS Bull.*, vol. 41, no. 10, pp. 765–774, 2016.

[6]   J. Ma, I. Karaman, and R. D. Noebe, "High temperature shape memory alloys," *Int. Mater. Rev.*, vol. 55, no. 5, pp. 257–315, 2010.

[7]   J. Mabe, F. Calkins, and G. Butler, "Boeing's Variable Geometry Chevron, Morphing Aerostructure for Jet Noise Reduction," *47th AIAA/ASME/ASCE/AHS/ASC Struct. Struct. Dyn. Mater. Conf. 14th AIAA/ASME/AHS Adapt. Struct. Conf. 7th*, no. May, pp. 1–19, 2006.

[8]   K. Otsuka and C. M. Wayman, *Shape Memory Materials*, vol. 119, no. 2. Cambridge University Press, 1998.

[9]   R. E. . Hirth, J. P. . Rogers, and H. C. Reed-Hill, *Deformation Twinning*, vol. 39, no. 1. 1964.

[10]   Y. Liu and H. Yang, "Strain dependence of the Clausius-Clapeyron relation for thermoelastic martensitic transformations in NiTi," *Smart Mater. Struct.*, vol. 16, no. 1, 2007.

[11]   H. E. Karaca *et al.*, "Effects of nanoprecipitation on the shape memory and material properties of an Ni-rich NiTiHf high temperature shape memory alloy," *Acta Mater.*, vol. 61, no. 19, pp. 7422–7431, 2013.

[12]   B. Kockar, I. Karaman, J. I. Kim, Y. I. Chumlyakov, J. Sharp, and C. J. (Mike) Yu, "Thermomechanical cyclic response of an ultrafine-grained NiTi shape memory alloy," *Acta Mater.*, vol. 56, no. 14, pp. 3630–3646, 2008.

[13]   G. J. Schiller, "Additive manufacturing for Aerospace," *IEEE Aerosp. Conf. Proc.*, vol. 2015–June, 2015.

[14]   W. E. Frazier, "Metal additive manufacturing: A review," *J. Mater. Eng.*

Perform., vol. 23, no. 6, pp. 1917–1928, 2014.

[15]   M. Elahinia, N. Shayesteh Moghaddam, M. Taheri Andani, A. Amerinatanzi, B. A. Bimber, and R. F. Hamilton, "Fabrication of NiTi through Additive Manufacturing: A Review," *Prog. Mater. Sci.*, vol. 83, pp. 630–663, 2016.

[16]   M. R. Hassan, M. Mehrpouya, and S. Dawood, "Review of the Machining Difficulties of Nickel-Titanium Based Shape Memory Alloys," *Appl. Mech. Mater.*, vol. 564, no. June, pp. 533–537, 2014.

[17]   M. H. Elahinia, M. Hashemi, M. Tabesh, and S. B. Bhaduri, "Manufacturing and processing of NiTi implants: A review," *Prog. Mater. Sci.*, vol. 57, no. 5, pp. 911–946, 2012.

[18]   M. H. Wu, "Fabrication of Nitinol Materials and Components," *Mater. Sci. Forum*, vol. 394–395, pp. 285–292, 2002.

[19]   C. Haberland, J. Walker, and J. Frenzel, "Additive Manufacturing of Shape Memory Devices and Pseudoelastic Components," in *Proceedings of the ASME 2013 Conference on Smart Materials, Adaptive Structures and Intelligent Systems*, 2013, pp. 1–8.

[20]   S. X.-D. Karamichailidou and G. Haidemenopoulos, "The Unique Properties , Manufacturing Processes and Applications of Near Equatomic Ni-Ti Alloys," *Univ. Thessaly Dep. Mech. Eng. Lab. Mater.*, 2016.

[21]   J. Ma *et al.*, "Spatial Control of Functional Response in 4D-Printed Active Metallic Structures," *Sci. Rep.*, vol. 7, p. 46707, 2017.

[22]   S. Dadbakhsh, M. Speirs, J. P. Kruth, J. Schrooten, J. Luyten, and J. Van Humbeeck, "Effect of SLM parameters on transformation temperatures of shape memory nickel titanium parts," *Adv. Eng. Mater.*, vol. 16, no. 9, pp. 1140–1146, 2014.

[23]   S. Bland and N. T. Aboulkhair, "Reducing porosity in additive manufacturing," *Met. Powder Rep.*, vol. 70, no. 2, pp. 79–81, 2015.

[24]   E. R. Denlinger, J. C. Heigel, P. Michaleris, and T. A. Palmer, "Effect of inter-layer dwell time on distortion and residual stress in additive manufacturing of titanium and nickel alloys," *J. Mater. Process. Technol.*, vol. 215, pp. 123–131, 2015.

[25]   S. Kou, *Welding Metallurgy*. John Wiley & Sons, 2003.

[26]   C. Haberland, M. Elahinia, J. M. Walker, H. Meier, and J. Frenzel, "On the development of high quality NiTi shape memory and pseudoelastic parts by additive manufacturing," *Smart Mater. Struct.*, vol. 23, no. 10, p. 104002, 2014.

[27]   T. Habijan *et al.*, "The biocompatibility of dense and porous Nickel-Titanium produced by selective laser melting," *Mater. Sci. Eng. C*, vol. 33, no. 1, pp. 419–

426, 2013.

[28] S. Dadbakhsh, B. Vrancken, J. P. Kruth, J. Luyten, and J. Van Humbeeck, "Texture and anisotropy in selective laser melting of NiTi alloy," *Mater. Sci. Eng. A*, vol. 650, pp. 225–232, 2016.

[29] S. Saedi, A. S. Turabi, M. T. Andani, N. S. Moghaddam, M. Elahinia, and H. Karaca, "Texture, aging, and superelasticity of selective laser melting fabricated Ni-rich NiTi alloys," *Mater. Sci. Eng. A*, vol. 686, no. January, pp. 1–10, 2017.

[30] B. A. Bimber, R. F. Hamilton, J. Keist, and T. A. Palmer, "Anisotropic microstructure and superelasticity of additive manufactured NiTi alloy bulk builds using laser directed energy deposition," *Mater. Sci. Eng. A*, vol. 674, pp. 125–134, 2016.

[31] G. S. Firstov, J. Van Humbeeck, and Y. N. Koval, "High-temperature shape memory alloys Some recent developments," *Mater. Sci. Eng. A*, vol. 378, no. 1–2 SPEC. ISS., pp. 2–10, Jul. 2004.

[32] G. S. Firstov, J. Van Humbeeck, and Y. N. Koval, "High temperature shape memory alloys problems and prospects," *J. Intell. Mater. Syst. Struct.*, 2006.

[33] B. Kockar, I. Karaman, J. I. Kim, and Y. Chumlyakov, "A method to enhance cyclic reversibility of NiTiHf high temperature shape memory alloys," *Scr. Mater.*, 2006.

[34] G. S. Bigelow, A. Garg, S. A. Padula, D. J. Gaydosh, and R. D. Noebe, "Load-biased shape-memory and superelastic properties of a precipitation strengthened high-temperature Ni50.3Ti29.7Hf20 alloy," *Scr. Mater.*, vol. 64, no. 8, pp. 725–728, 2011.

[35] L. C. Meng, X.L.; Zheng, Y.F.; Wang, Z.; Zhao, "Effect of aging on the phase transformation and mechanical behavior of Ti36Ni49Hf15 high temperature shape memory alloy," *Scr. Mater.*, vol. 42, pp. 341–348, 2000.

[36] O. Karakoc *et al.*, "Effects of upper cycle temperature on the actuation fatigue response of NiTiHf high temperature shape memory alloys," *Acta Mater.*, vol. 138, pp. 185–197, 2017.

[37] O. Karakoc, C. Hayrettin, D. Canadinc, and I. Karaman, "Role of applied stress level on the actuation fatigue behavior of NiTiHf high temperature shape memory alloys," *Acta Mater.*, 2018.

[38] S. Saedi, A. S. Turabi, M. T. Andani, C. Haberland, H. Karaca, and M. Elahinia, "The influence of heat treatment on the thermomechanical response of Ni-rich NiTi alloys manufactured by selective laser melting," *J. Alloys Compd.*, vol. 677, pp. 204–210, 2016.

[39] B. E. Franco *et al.*, "A Sensory Material Approach for Reducing Variability in Additively Manufactured Metal Parts," *Sci. Rep.*, vol. 7, no. 1, pp. 1–12, 2017.

[40] J. Sam, B. Franco, J. Ma, I. Karaman, A. Elwany, and J. H. Mabe, "Tensile actuation response of additively manufactured nickel-titanium shape memory alloys," *Scr. Mater.*, vol. 146, pp. 164–168, 2018.

[41] N. T. Aboulkhair, N. M. Everitt, I. Ashcroft, and C. Tuck, "Reducing porosity in AlSi10Mg parts processed by selective laser melting," *Addit. Manuf.*, vol. 1, pp. 77–86, 2014.

[42] B. Kockar, I. Karaman, A. Kulkarni, Y. Chumlyakov, and I. V. Kireeva, "Effect of severe ausforming via equal channel angular extrusion on the shape memory response of a NiTi alloy," *J. Nucl. Mater.*, vol. 361, no. 2–3 SPEC. ISS., pp. 298–305, 2007.

[43] R. Santamarta *et al.*, "TEM study of structural and microstructural characteristics of a precipitate phase in Ni-rich Ni-Ti-Hf and Ni-Ti-Zr shape memory alloys," *Acta Mater.*, 2013.
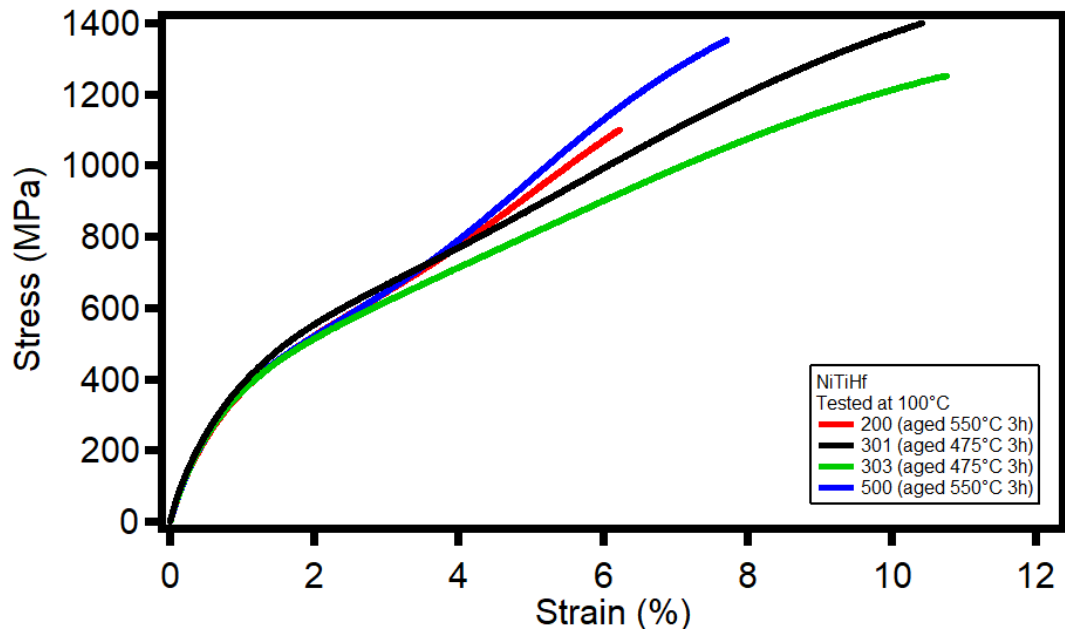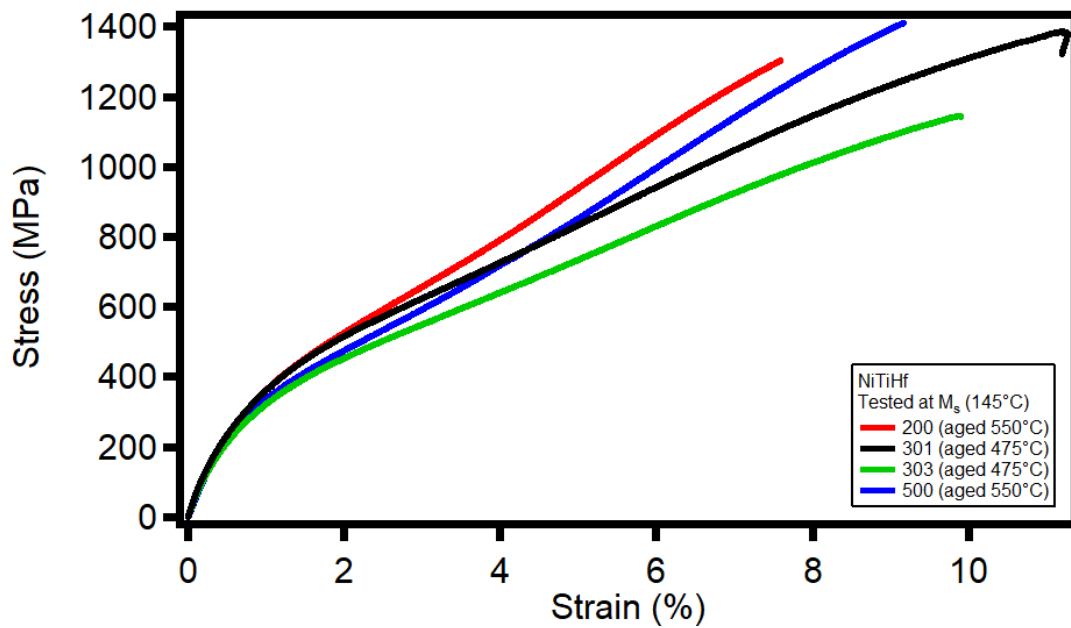
Figure 32. Stress vs. strain of NiTiHf at 100°C

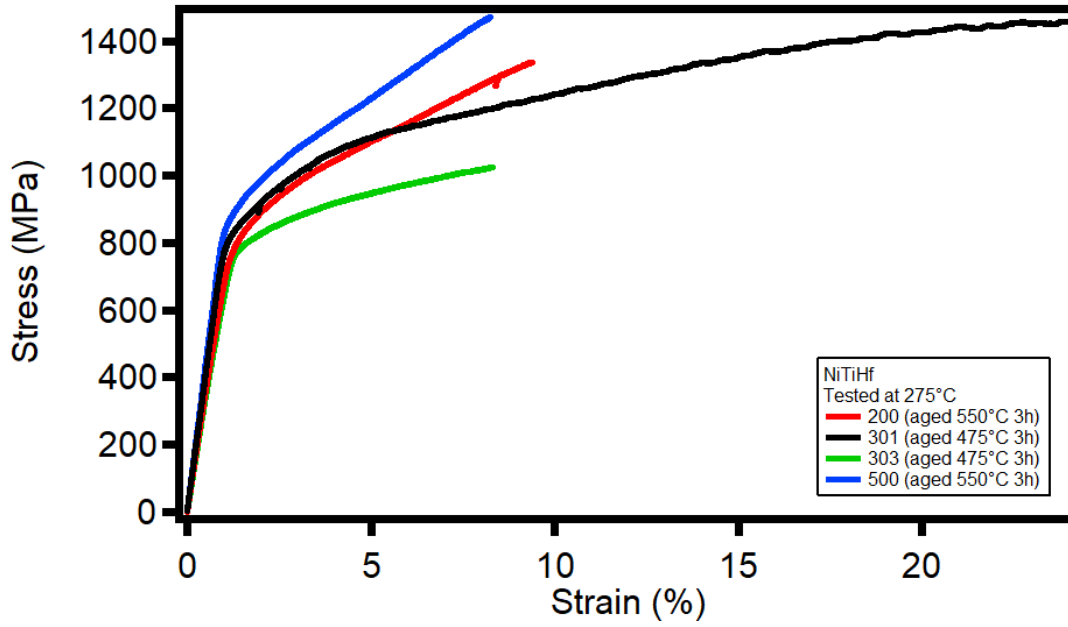**Figure 33.** Stress vs. strain of NiTiHf at 145°C

Figure 34. Stress vs. strain of NiTiHf at 275°C
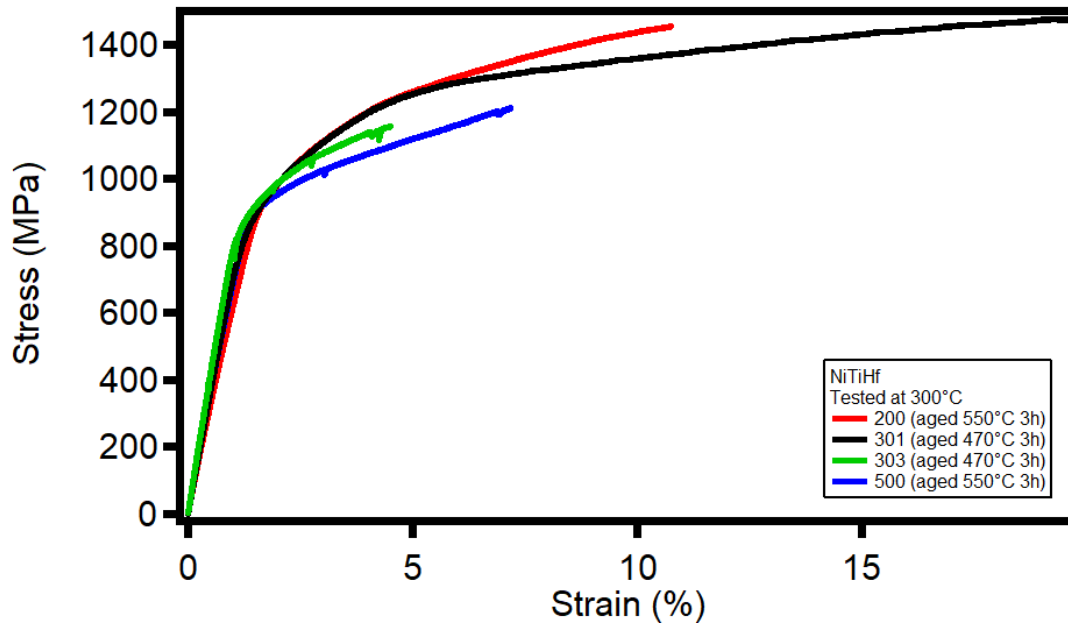

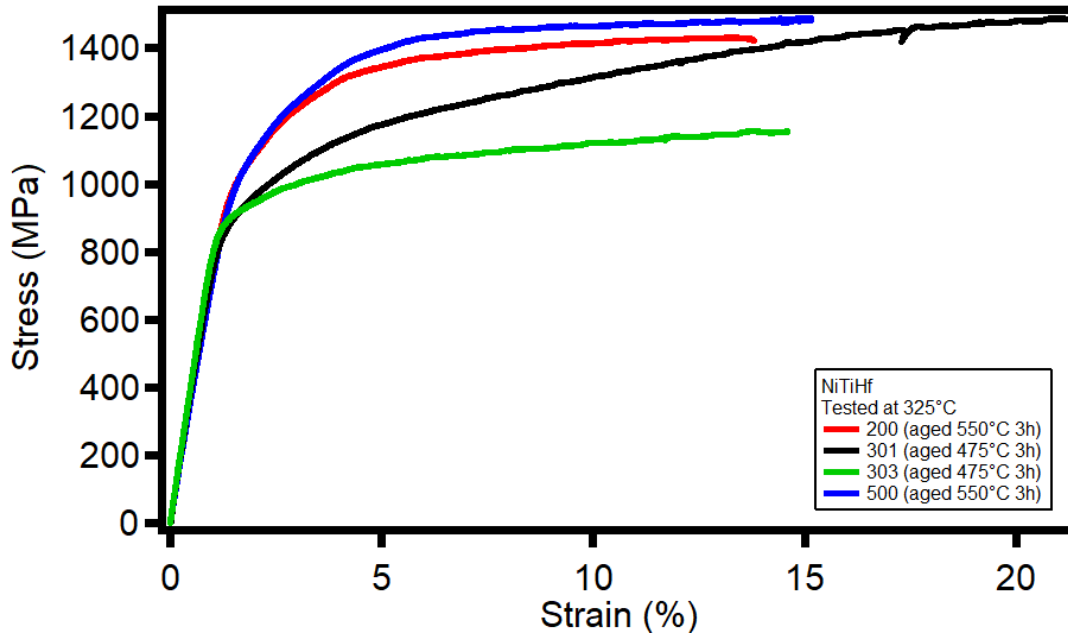**Figure 35.** Stress vs. strain of NiTiHf at 300°C
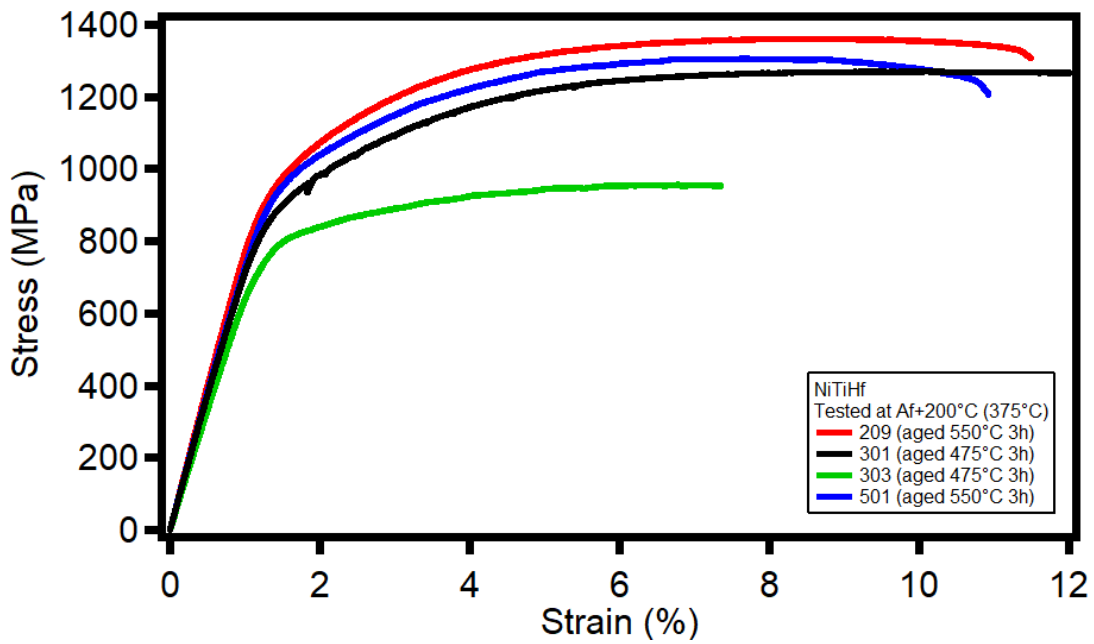
Figure 36. Stress vs. strain of NiTiHf at 325°C

Figure 37. Stress vs. strain of NiTiHf at 375°C